

Local Plaquette Physics as Key Ingredient of High-Temperature Superconductivity in Cuprates

Michael Danilov,¹ Erik G. C. P. van Loon,^{2,3,4,*} Sergey Brener,^{1,5} Sergei Iskakov,^{6,7} Mikhail I. Katsnelson,^{8,7} and Alexander I. Lichtenstein^{1,5,7,†}

¹*Institute of Theoretical Physics, University of Hamburg, 20355 Hamburg, Germany*

²*Institut für Theoretische Physik, Universität Bremen, Otto-Hahn-Allee 1, 28359 Bremen, Germany*

³*Bremen Center for Computational Materials Science, Universität Bremen, Am Fallturm 1a, 28359 Bremen, Germany*

⁴*Department of Physics, Lund University, Professorsgatan 1, 223 63, Lund, Sweden*

⁵*The Hamburg Centre for Ultrafast Imaging, Luruper Chaussee 149, 22761 Hamburg, Germany*

⁶*Department of Physics, University of Michigan, Ann Arbor, Michigan 48109, USA*

⁷*Theoretical Physics and Applied Mathematics Department,*

Ural Federal University, Mira Str.19, 620002, Yekaterinburg, Russia

⁸*Radboud University, Institute for Molecules and Materials, 6525AJ Nijmegen, The Netherlands*

A major pathway towards understanding complex systems is given by exactly solvable reference systems that contain the essential physics of the system. For the $t - t' - U$ Hubbard model, the four-site plaquette is known to have a point in the $U - \mu$ space where states with electron occupations $N = 2, 3, 4$ per plaquette are degenerate [Phys. Rev. B **94**, 125133 (2016)]. We show that such a critical point in the lattice causes an instability in the particle-particle singlet d-wave channel and manifests some of the essential elements of the cuprate superconductivity. For this purpose we design an efficient superperturbation theory – based on the dual fermion approach – with the critical plaquette as the reference system. Thus, the perturbation theory already contains the relevant d-wave fluctuations from the beginning via the two-particle correlations of the plaquette. We find that d-wave superconductivity remains a leading instability channel under reasonably broad range of parameters. The next-nearest-neighbour hopping t' is shown to play a crucial role in a formation of strongly bound electronic bipolarons whose coherence at lower temperature results in superconductivity. The physics of the pseudogap within the developed picture is also discussed.

I. INTRODUCTION

After 35 years since the discovery of the high-temperature superconductivity¹, there is still no consensus on the nature of the mechanism of d-wave pairing in cuprates^{2–7}. Nevertheless, new experimental findings clearly point to the existence of a quantum critical point around a hole doping of $\delta \approx 0.24$ ^{8–10}. This concentration separates the exotic bad-metal state for smaller doping from Fermi-liquid behaviour for larger hole concentration with “normal” Fermi-surface described, at least qualitatively, by conventional density-functional theory¹¹. Moreover, the carrier density obtained from Hall effect measurements in large-doping regime is equal to its nominal value $n_H \approx 1 - \delta$ while for smaller doping the bad-metal behaviour appears with Fermi-arcs, “enigmatic pseudogap phase” and ($n_H \approx \delta$) at high temperature^{8,12}. Recent investigations of highly overdoped cuprates show that this “strange metal phase” is located around $\delta_c \approx 0.24$ point⁹. For hole concentrations less than δ_c superconducting pairs come entirely from the region of incoherent electrons at the antinode region (X-point) of the Brillouin zone (Planckian dissipators)⁹.

Electronic specific heat measurements for many different cuprate superconductors reveal in a normal phase a huge peak in the electron Density of States (DOS) at the Fermi energy at $\delta_c \approx 0.24$ with a strong evidence of the presence of a Quantum Critical Point (QCP) at this hole doping⁸. Taking into account this critical concentration as a fingerprint of high-Tc materials, we formulate a simple strong coupling theory of the electronic instability based on cluster dual-fermion superperturbation theory^{13,14}.

First-principle electronic structure calculations¹¹ suggest that a single-band tight-binding model with next nearest neighbour (NNN) hopping and on-site Coulomb interaction, the so-called “ $t - t' - U$ ” Hubbard model, has all ingredients to describe high-Tc phenomena. Moreover, the case of $t'/t = -0.15$ corresponds to the LSCO-cuprate family while one expects $t'/t = -0.3$ to describe cuprate families with higher T_c such as e.g. YBCO and Tl2201¹⁵. We developed an efficient second-order perturbation theory starting from a 2×2 plaquette, where $\delta = 0.25$ corresponds to a highly degenerate point for $U/t \approx 6$ ¹⁶. In a close analogy with the Kondo model, where the degeneracy of the two spin states of a magnetic impurity plays a crucial role in the anomalous low-energy properties, the special properties of the degenerate states of the plaquette can reveal the nature of the anomalous behavior of the interacting Hubbard model on a two-dimensional lattice.

The first attempt to discuss the plaquette physics as the main ingredient of the high-Tc theory was done with the cluster dynamical mean-field theory (DMFT) scheme¹⁷, and later Altman and Auerbach analytically explained the importance of plaquette two-hole states with $d_{x^2-y^2}$ symmetry¹⁸. Nevertheless they did not consider the possibility of a degenerate ground state of the plaquette¹⁶ with a correspondingly divergent perturbation series similar to the perturbative theory in Kondo problem¹⁹. In some sense, the degeneracy of the ground states with $N = 2, 3, 4$ electrons per plaquette in the critical point plays the same role as the degeneracy between spin-up and spin-down states in the conventional Kondo effect and is crucially important for the pseudogap

formation¹⁶. If we treat the Kondo problem in dual perturbation from the atomic limit²⁰ then the local four-point vertex is divergent at low temperature, while the Green's function is finite. In the case of degenerate plaquette both Green's function for reference system and vertex are divergent for low temperature.

We will start with this six-fold degenerate ground state of a 2×2 plaquette with t'/t fixed to -0.15 depicted as a star-point in the Fig. 1. Since we use here periodic boundary conditions the critical Coulomb interaction for plaquette degenerate point becomes $U/t = 5.56$ in contrast with the case of isolated plaquette¹⁶. This is in a very good agreement with the value of the Coulomb interaction $U/t = 5.6$ that was found in the diagrammatic Monte Carlo calculations²¹ in a search of pseudogap formation, and the value of $U/t \approx 6$ pointed out in the recent review⁸ as the most reasonable value of the effective Hubbard interaction for cuprates. Note also that periodic boundary conditions effectively double t' compared to t , which explains the chosen value of the NNN hopping twice smaller than in Ref.¹⁶. At a special value of the chemical potential¹⁶ $\mu \approx 0.48$ the ground state for the half-filled $N = 4$ antiferromagnetic singlet is degenerate with the singlet for $N = 2$ electrons and with two doublets from $N = 3$ sector. For these values of the parameters the plaquette state corresponds to the hole doping of $\delta_c = 0.25$. If we start from such a degenerate point as a reference system, any perturbation theory for the lattice will be highly divergent.

We will also consider reference systems differing from the degenerate point in the value of the chemical potential. For smaller $\mu \approx 0$ (marked with the circle in Fig. 1) the lattice would tend to a metallic behavior, for larger $\mu \approx 0.8$ (marked with the square) the perturbation for the lattice results in a superconducting $d_{x^2-y^2}$ instability.

Facing such a complex system that is hard to solve exactly, it is frequently useful to consider solvable reference systems instead. This strategy is the basis for variational and mean-field approaches, among others. The simplest exactly solvable model is based on infinite-dimensional case with a plaquette as elementary unit (cluster DMFT)²². However, nonlocal correlations effects should be relevant for the low-dimensional systems which means that we have to go beyond this limiting case. In electronic systems, the dual fermion²³ approach provides a recipe for using arbitrary local reference systems²⁴, with a way to incorporate nonlocal corrections in a systematic fashion. There is a large amount of freedom in choosing this reference system which can be used to capture essential physics of the full system under investigation.

In the case of the doped $t-t'-U$ Hubbard model, d-wave superconducting fluctuations are known to be important, and a four-site plaquette is the minimal reference system that contains their spatial structure and additionally has an important degenerate point^{16,25}. Below we show that this degenerate point also induces clear signatures in the two-particle correlation function, which is the basic building block of the dual fermion perturbation theory.

The central question for a reliable theory of the high- T_c cuprates can be formulated in the following manner: what is the mechanism of superconducting coupling and which minimal model explains the key experimental observations such as nodal-antinodal dichotomy and pseudogap formation in the underdoped regime, strange metal behaviour, etc.? An important part of that question is: what is the minimal length scale needed to understand these phenomena? For the Mott insulating phase, a single atom with Coulomb interaction, coupled to a (dynamical) bath, is qualitatively sufficient. Extending this to a single bond explains how antiferromagnetic exchange interactions between local moments emerge. It has been argued, starting from Ref.¹⁷, that a plaquette consisting of 2×2 sites is the minimal unit when thinking about d-wave superconductivity: it is sufficiently large to express the phase difference in the horizontal and vertical direction that characterizes d-wave superconductivity. The $t-t'-U$ plaquette is known to have a critical line of degenerate states in parameter space of (U, t', μ) ²⁵. We will argue that, similar to how the generation of antiferromagnetic exchange on a single bond forms the starting point for antiferromagnetism, this plaquette degeneracy plays a central role in the origin of d-wave superconductivity.

II. DUAL FERMION APPROACH WITH A GENERAL REFERENCE SYSTEM

We start with a general lattice fermion model with the local Hubbard-like interaction vertex U . Generalisation to the multi-orbital case with general interactions is straightforward²⁶. The general strategy of the dual fermion approach is related to formally exact separation of the local and non-local correlations effects. We introduce auxiliary dual fermionic fields which will couple local correlated impurities or clusters back to the original lattice²³.

Using the path-integral formalism the partition function of a general fermionic lattice system can be written in the form of the functional integral over Grassmann variables $[c^*, c]$:

$$Z = \int \mathcal{D}[c^*, c] \exp(-S_L[c^*, c]) \quad (1)$$

The original action of interacting lattice fermions S_L can be expressed as the sum of the one-electron contribution and the interaction term. The former is most conveniently represented in Matsubara and momentum space, using the Fourier transformed hopping matrix $\hat{t}_{\mathbf{k}}$ (in the single-orbital case, this provides the energy spectrum), whereas the Hubbard interaction U is local and

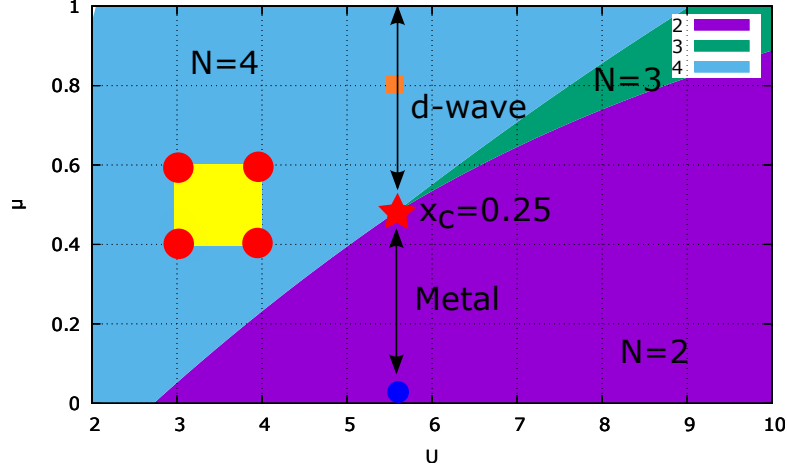


FIG. 1. Phase diagram of 2×2 plaquette for different particle sectors ($N = 2, 3, 4$) and zero temperature with the degenerate point marked by star. The circle and square display the shifted chemical potentials for a test comparison. The region of $d_{x^2-y^2}$ superconducting phase and normal metal for square lattice are also marked.

instantaneous and is therefore treated in imaginary time and real space. Any type of local multi-orbital interaction is allowed.

$$S_L[c^*, c] = - \sum_{\mathbf{k}\nu\sigma} c_{\mathbf{k}\nu\sigma}^* [i\nu + \mu - \hat{t}_{\mathbf{k}}] c_{\mathbf{k}\nu\sigma} + \sum_i \int_0^\beta d\tau U n_{i\tau\uparrow}^* n_{i\tau\downarrow}. \quad (2)$$

Here and in the following, $\nu = (2n+1)\pi/\beta$ ($\omega = 2n\pi/\beta$), with $n \in \mathbb{Z}$, are the fermionic (bosonic) Matsubara frequencies, β is the inverse temperature, τ is the imaginary time in the interval $[0, \beta]$, μ is the chemical potential, the index i labels the lattice sites, m can refer to different orbitals inside plaquette (\hat{t} can be a matrix in orbital space), σ is the spin projection and the \mathbf{k} -vectors are quasimomenta. In order to keep the notation simple, it is useful to introduce the combined index $|1\rangle \equiv |i, m, \sigma, \tau\rangle$ while assuming summation over repeated indices. Summation over Matsubara frequencies ν assume normalization factor $1/\beta$ and the \mathbf{k} integration normalized by volume of Brillouin zone. Translational invariance is assumed for simplicity in the following, although a real space formulation is possible²⁷.

In order to formulate an expansion around a suitable reference action, as illustrated in Fig. 2, a quantum cluster problem is introduced by a general frequency dependent hybridization function $\hat{\Delta}_\nu$ and the same local interaction,

$$S_\Delta[c_i^*, c_i] = - \sum_{\nu, \sigma} c_{i\nu\sigma}^* [i\nu + \mu - \hat{\Delta}_\nu] c_{i\nu\sigma} + \sum_\nu U n_{i\nu\uparrow}^* n_{i\nu\downarrow}. \quad (3)$$

$\hat{\Delta}_\nu$ in this notation is the plaquette-local effective "hybridization" matrix which describes hoppings inside the cluster as well connections to an auxiliary fermionic bath. Note that $\hat{\Delta}_\nu$ is allowed to contain instantaneous parts, i.e., finite asymptotic for $\nu \rightarrow \infty$. The main motivation for rewriting the lattice action in terms of a quantum cluster model is that such a reference system can be solved numerically exactly for a given hybridization function using Exact Diagonalization (ED) or continuous time Quantum Monte Carlo (CT-QMC)²⁸. In this work, we use an isolated cluster as a reference model. In that case, Δ is completely instantaneous and the model is solvable by ED.

Using the locality of the hybridization function $\hat{\Delta}_\nu$, the lattice action Eq. (2) can be rewritten exactly in terms of the individual impurity models and the effective one-electron coupling ($\hat{\Delta}_\nu - \hat{t}_{\mathbf{k}}$) between different impurities (or plaquettes):

$$S_L[c^*, c] = \sum_i S_\Delta[c_i^*, c_i] + \sum_{\mathbf{k}\nu\sigma} c_{\mathbf{k}\nu\sigma}^* (\hat{t}_{\mathbf{k}} - \hat{\Delta}_\nu) c_{\mathbf{k}\nu\sigma} \quad (4)$$

Although we can solve an individual impurity model exactly, in the present formulation the effect of spatial correlations due to the second term in Eq.(4) is still problematic, since the impurity action is non-Gaussian and one cannot use the Wick's theorem. The main idea of the dual fermion transformation is the change of variables from strongly correlated fermions (c^*, c) to weakly correlated "dual" Grassmann fields (d^*, d) in the path integral representation for the partition function from Eq. (1), followed by a simple perturbation treatment. The new "dual" variables are introduced through the following Hubbard-Stratonovich (HS)-transformation^{29,30} with the following single-particle matrix $\tilde{t}_{\mathbf{k}\nu} = (\hat{t}_{\mathbf{k}} - \hat{\Delta}_\nu)$.

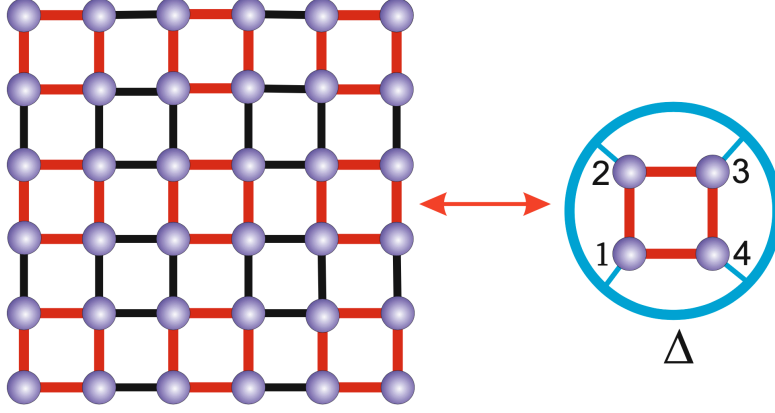


FIG. 2. Schematic representation of a plaquette reference system for the square lattice.

$$e^{-c_1^* \tilde{t}_{12} c_2} = \det[-\tilde{t}] \int \mathcal{D}[d^*, d] e^{d_1^* \tilde{t}_{12}^{-1} d_2 - d_1^* c_1 - c_1^* d_1} \quad (5)$$

We can immediately see this HS-transformation “localizes” the $[c_i^*, c_j]$ fermions: while on the left hand-side they are still “hopping” through the lattice, on the right-hand side they are localized on one site $[c_i^*, c_i]$.

Compared to the original dual fermion scheme²³, we perform the Hubbard-Stratonovich decoupling here without any scaling factors related with local Green’s function in order to reduce the number of matrix multiplications in the final algorithm³¹. In this way, the notation of the formalism becomes closer to the original strong-coupling expansion^{32–36}. Nevertheless, we would like to stress that the dual fermion theory includes a freedom to choose an arbitrary hybridisation function $\hat{\Delta}_v$.

With this reference system, the lattice partition function becomes

$$\frac{Z}{Z_d} = \int \mathcal{D}[c^*, c, d^*, d] \exp(-S[c^*, c, d^*, d]) \quad (6)$$

with $Z_d = \det[-\tilde{t}]$. The lattice action transforms to

$$S[c^*, c, d^*, d] = \sum_i S_{\Delta}^i - \sum_{\mathbf{k}, v, \sigma} d_{\mathbf{k}v\sigma}^* (\hat{t}_{\mathbf{k}} - \hat{\Delta}_v)^{-1} d_{\mathbf{k}v\sigma} \quad (7)$$

Hence the coupling between sites is transferred to a local coupling to the auxiliary fermions:

$$S_{\Delta}^i[c_i^*, c_i, d_i^*, d_i] = S_{\Delta}[c_i^*, c_i] + \sum_{v, \sigma} (d_{iv\sigma}^* c_{iv\sigma} + c_{iv\sigma}^* d_{iv\sigma}) \quad (8)$$

For the last term we use the invariance of the trace so that the sum over all states labeled by \mathbf{k} could be replaced by the equivalent summation over all sites by a change of basis in the second term. The crucial point is that the coupling to the auxiliary fermions is purely local and S_{Δ}^i decomposes into a sum of local terms. The lattice fermions can therefore be integrated out from S_{Δ}^i for each site i separately. This completes the change of variables:

$$\frac{1}{Z_{\Delta}} \int \mathcal{D}[c^*, c] \exp(-S_{\Delta}^i[c_i^*, c_i, d_i^*, d_i]) = \exp\left(-\sum_{v\sigma} d_{iv\sigma}^* g_v d_{iv\sigma} - V_i[d_i^*, d_i]\right) \quad (9)$$

where Z_{Δ} is partition function of impurity action Eq. (3) and g_v is the exact impurity Green function

$$g_{12} = -\langle c_1 c_2^* \rangle_\Delta = \frac{1}{Z_\Delta} \int \mathcal{D}[c^*, c] c_1 c_2^* e^{-S_\Delta[c^*, c]} \quad (10)$$

The above equation may be viewed as the defining equation for the dual potential $V[d^*, d]$. The choice of the dual transformation in the form of Eq.(5), without the traditional renormalization of the d -fields by a factor of g_v^{-1} , ensures a particularly simple form of this potential. The price that we pay for this simple form is the unconventional dimensionality of the dual Green's function and self-energy, but it proves to be very convenient for numerical multiorbital/cluster calculations. An explicit expression is found by expanding both sides of Eq. (9) and equating the resulting expressions order by order. Formally this can be done up to all orders and in this sense the transformation to the dual fermions is exact. For most applications, the dual potential is approximated by the first non-trivial interaction vertex:

$$V[d^*, d] = \frac{1}{4} \sum_{1234} \gamma_{1234}^P d_1^* d_2^* d_3 d_4 \quad (11)$$

where for the local vertex the combined index $1 \equiv \{mv\sigma\}$ comprises orbital degrees of freedom (or cluster sites), frequency, and spin. γ is the exact, fully antisymmetric, reducible two-particle vertex of the local quantum impurity problem, in the particle-particle notation (denoted by the index P). The absence of normalization in the HS-transformation (5) leads to the impurity “legs” remain “unamputated”. Normally this procedure implies division by the single-particle Green's functions. In the multiorbital case, this division involves a potentially unstable matrix inversion, which is avoided by the present choice of normalization. The vertex is then given by the connected part of the local two-particle correlations function

$$\gamma_{1234} = \kappa_{1234} - \kappa_{1234}^0 \quad (12)$$

with the two-particle Green's function, κ , of the local reference system being defined in particle-particle notation as :

$$\kappa_{1234}^P = \langle c_1 c_2 c_4^* c_3^* \rangle_\Delta = \frac{1}{Z_\Delta} \int \mathcal{D}[c^*, c] c_1 c_2 c_4^* c_3^* e^{-S_\Delta[c^*, c]} \quad (13)$$

The disconnected part, κ^0 , of the plaquette two-particle Green function reads

$$\kappa_{1234}^0 = g_{13} g_{24} - g_{14} g_{23} \quad (14)$$

The single- and two-particle Green functions can be calculated using the CT-QMC Monte Carlo algorithms²⁸. After integrating out the lattice fermions, the dual action depends on the new variables only

$$\tilde{S}[d^*, d] = - \sum_{\mathbf{k} \nu \sigma} d_{\mathbf{k} \nu \sigma}^* \tilde{G}_{0 \mathbf{k} \nu}^{-1} d_{\mathbf{k} \nu \sigma} + \sum_i V_i[d_i^*, d_i], \quad (15)$$

here the bare dual Green function is of the form

$$\tilde{G}_{\mathbf{k} \nu}^0 = \left[\left(\hat{t}_{\mathbf{k}} - \hat{\Delta}_\nu \right)^{-1} - g_\nu \right]^{-1}. \quad (16)$$

Action Eq.(15) allows us to calculate the dual self-energy, $\tilde{\Sigma}_{\mathbf{k} \nu}$ with a level of approximation of our choice. Once this is done, the results are transformed back using an exact relation between the dual and the lattice Green's functions (Appendix A).

The lattice self-energy is the sum of the reference contribution Σ^0 (i.e the self-energy of the impurity or the cluster) and the correction Σ' which is related to the dual self-energy $\tilde{\Sigma}$ in the following manner¹³

$$\begin{aligned} \Sigma_{\mathbf{k} \nu} &= \Sigma_\nu^0 + \Sigma'_{\mathbf{k} \nu} \\ \Sigma'_{\mathbf{k} \nu} &= g_\nu^{-1} - (g_\nu + \tilde{\Sigma}_{\mathbf{k} \nu})^{-1} \end{aligned} \quad (17)$$

For numerical calculations it is more convenient not to calculate the lattice self-energy, but to use directly a simple connection between the dual self-energy and the lattice Green's function²³

$$G_{\mathbf{k} \nu} = \left[\left(g_\nu + \tilde{\Sigma}_{\mathbf{k} \nu} \right)^{-1} - \tilde{t}_{\mathbf{k} \nu} \right]^{-1}. \quad (18)$$

where $\tilde{\Sigma}_{\mathbf{k} \nu}$ is calculated via diagrammatic perturbation scheme using the $\tilde{G}_{0 \mathbf{k} \nu}^{-1}$ matrix and plaquette vertex γ_{1234} . The properly rescaled dual self energy plays the role of a T-matrix for the reference Green's function g . With this relation, the calculation only involves single and two-particle correlation functions of the reference system and no “amputated” quantities. By avoiding many matrix inversions, this makes it suitable for multi-orbital systems. The case of the “bare dual fermions” $\tilde{\Sigma}_{\mathbf{k} \nu} = 0$ is equivalent to the cluster perturbation theory³⁷.

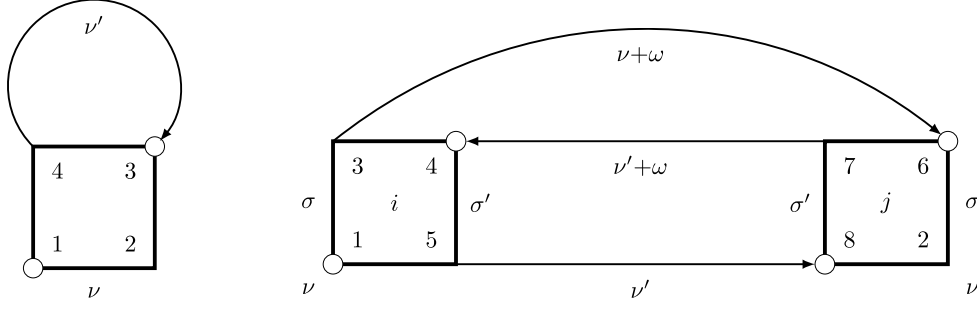


FIG. 3. Feynman diagram for the first order (left) and the second order (right) dual fermion perturbation for the self-energy $\tilde{\Sigma}$: a line represents the non-local \tilde{G}_{43} and a box is the local γ_{1234} .

III. PERTURBATION IN DUAL SPACE

The cluster dual fermion perturbation theory (Fig. 2) starts with the interaction between dual fermions. We use here the particle-hole notation for the local vertex and write explicit spin indices and Matsubara frequency structure of the connected two particle Green's function^{23,38} as follows:

$$-\gamma_{1234}^{\sigma\sigma'}((\nu, \nu'), \omega) = \langle c_{1\sigma}(\nu)c_{2\sigma'}^*(\nu + \omega)c_{3\sigma'}(\nu' + \omega)c_{4\sigma}^*(\nu') \rangle_{\Delta} - \beta g_{12}^{\sigma}(\nu)g_{34}^{\sigma'}(\nu')\delta_{\omega 0} + \beta g_{14}^{\sigma}(\nu)g_{32}^{\sigma'}(\nu + \omega)\delta_{\nu\nu'}\delta_{\sigma\sigma'}. \quad (19)$$

In Matsubara space, the vertex depends on two fermionic (ν, ν') and one bosonic (ω) frequencies. For the sake of completeness and the reader's convenience we mention that the connection between the particle-particle and the particle-hole notation reads $\gamma_{1234}(\nu, \nu', \omega) = \gamma_{1342}^p(\nu, \nu', \nu + \nu' + \omega)$ with the particle-particle frequency notation being $\kappa_{1234}^p(\nu, \nu', \omega) = \langle c_1(\nu)c_2(\omega - \nu)c_4^*(\omega - \nu')c_3^*(\nu') \rangle_{\Delta}$. Thus, the bare vertex of the dual fermion perturbation theory is the full connected correlation function of the reference system. The present vertex differs from the usual dual fermion expression due to the different rescaling factor of the Hubbard-Stratonovich field. Here, we avoid amputation of the legs of the vertex, which requires division by Green's functions at all external points.

It is useful to symmetrize the vertex into charge density (d) and magnetic (m) channels:

$$\gamma_{1234}^{d/m}(\nu, \nu', \omega) = \gamma_{1234}^{\uparrow\uparrow}(\nu, \nu', \omega) \pm \gamma_{1234}^{\uparrow\downarrow}(\nu, \nu', \omega)$$

Now we can write the first-order dual fermion self-energy which is local in plaquette space (Fig. 3):

$$\tilde{\Sigma}_{12}^{(1)i}(\nu) = \sum_{\nu', 3, 4} \gamma_{1234}^d(\nu, \nu', 0) \tilde{G}_{43}^{ii}(\nu') \quad (20)$$

The second order Feynman diagram for DF-perturbation (Fig. 3) in real space (\mathbf{R}_{ij}) has density- and magnetic-channel contributions with corresponding constants ($c_d = -\frac{1}{4}$ and $c_m = -\frac{3}{4}$):

$$\tilde{\Sigma}_{12}^{(2)ij}(\nu) = \sum_{\nu'} \sum_{3-8} \sum_{\alpha=d, m} c_{\alpha} \gamma_{1345}^{\alpha, i}(\nu, \nu', \omega) \tilde{G}_{36}^{ij}(\nu + \omega) \tilde{G}_{74}^{ji}(\nu' + \omega) \tilde{G}_{58}^{ij}(\nu') \gamma_{8762}^{\alpha, j}(\nu', \nu, \omega) \quad (21)$$

In principle, one can go beyond the second order perturbation expansion and include dual ladder diagrams^{38,39}, dual parquet diagrams⁴⁰ or a stochastic sum of all dual diagrams with the two-particle vertex γ_{1234} , using diagrammatic Monte Carlo in dual space⁴¹⁻⁴³. In addition, the diagrammatic series can be made self-consistent, using dual skeleton diagrams and “bold” lines. Finally, one can also update the reference system (and obtain a frequency dependent Δ) with quite involved numerical approach. But as the main goal of the present work is not to present quantitatively reliable results but rather to highlight the connection between the degenerate reference system and the superconducting fluctuations we will mostly stick to the second-order consideration. The calculations shown here were performed using a Fortran implementation of dual fermions that uses the equivalence of the four sites in the plaquette to speed up the vertex calculation. The results were checked against an open source implementation of the second-order dual fermion perturbation^{31,44}, based on TRIQS⁴⁵ and with pomero⁴⁶ as an impurity solver as well as cross-checked with the momentum-space cluster dual-fermion scheme⁴⁷.

IV. RESULTS FOR PLAQUETTE DUAL SCHEME

We study the optimally doped square lattice Hubbard model, with nearest neighbour hopping t and NNN hopping t' . As illustrated in Fig. 2, the original lattice can be reconsidered as a lattice of 2×2 plaquettes. Every unit cell of the plaquette lattice

contains 4 atoms of the original lattice, as shown on the left-hand side of Fig. 2. The plaquette lattice has the following 4×4 hopping matrix (see Fig. 2),

$$t_{\mathbf{k}} = \begin{pmatrix} \varepsilon & tK^{0+} & t'L^{-+} & tK^{-0} \\ tK^{0-} & \varepsilon & tK^{-0} & t'L^{--} \\ t'L^{+-} & tK^{+0} & \varepsilon & tK^{0-} \\ tK^{+0} & t'L^{++} & tK^{0+} & \varepsilon \end{pmatrix} \quad (22)$$

where the functions $K_{\mathbf{k}}^{mn}$ and $L_{\mathbf{k}}^{mn}$, with $m, n \in \{-1, 0, +1\}$, are defined as

$$K_{\mathbf{k}}^{mn} = 1 + e^{i(mk_x + nk_y)} \\ L_{\mathbf{k}}^{mn} = 1 + e^{i(mk_x + nk_y)} + e^{imk_x} + e^{ink_y}$$

We will use a single plaquette as the reference system. Compared to the single-site dual fermion formalism, this plaquette reference system already encompasses the short-ranged correlations that are essential in this system.

In the dual fermion approach, there is a general freedom of choosing the most appropriate reference system. One way to construct a plaquette reference system would be to simply remove all black links in Fig. 2 (and attach the remaining sites to a bath). This is equivalent to the self-consistent cluster-DMFT scheme¹⁷ and corresponds to averaging over the supercell Brillouin zone. This scheme, however, eliminates exactly half of the nearest-neighbor hoppings and three quarters of the next-nearest-neighbor hoppings.

Here we choose another path and consider plaquettes with periodic boundary conditions as a static reference system. In terms of the supercell Brillouin zone, this corresponds to achieving self-consistency for $k = 0$ only, instead of the momentum average. The intra-plaquette hopping reads

$$\Delta_0 \equiv t_{\mathbf{k}=0} = \begin{pmatrix} \varepsilon_0 & 2t & 4t'_0 & 2t \\ 2t & \varepsilon_0 & 2t & 4t'_0 \\ 4t'_0 & 2t & \varepsilon_0 & 2t \\ 2t & 4t'_0 & 2t & \varepsilon_0 \end{pmatrix}. \quad (23)$$

Note that we include the possibility of using a different chemical potential $\mu_0 = -\varepsilon_0$ in the reference system, compared to that of the lattice model $\mu = -\varepsilon$ to adjust the hole doping to about $\delta = 0.15$. We fix the nearest neighbour hopping t but retain the freedom of adjusting the next nearest neighbour hopping t' in the dual fermion transformation. For example this may be used to reduce the factor 4 for the t' hoppings for the periodic boundary conditions for 2×2 plaquette if we chose $t'_0 = t'/2$.

With the plaquette as the reference system, one can use the exact diagonalization approach to calculate the dual Green's function and the plaquette vertex function⁴⁸. We choose the optimal parameters for the High- T_c cuprates where the ground state of the plaquette is six-fold degenerate¹⁶ with $U = 5.56$, $t = -1$, $t'_0 = 0.15$, $\mu_0 = 0.48$ with $t' = 0.15$ or 0.3 and $\mu = 0.7$ or 1.5 correspondingly to keep the optimal doping $\delta \approx 0.15$ in the lattice. We investigate different temperatures as low as possible until the dual perturbation theory breaks down due to the divergence in the plaquette vertex function at the degenerate point in the limit $T \rightarrow 0$.

In Fig. 4 we compare the density of states (DOS) for plaquette DF second-order perturbation (DF2) with the so-called cluster perturbation theory (CPT) which corresponds to zero dual-self energy in Eq.(18) for quite high temperature ($\beta = 3$). We use Padé-analytical continuation from Matsubara to the real energy axes⁴⁹. One can see that the DOS for the dual fermion theory is much more sharply peaked near the Fermi level compared to the CPT-result. For comparison we also show the ED result for the plaquette with a sharp peak exactly at Fermi level due to six-fold degenerate ground state. In this case there is still no signature for a pseudogap and the lattice self-energy is “well-behaved”.

A. Vertex and Bethe–Salpeter Equation

The central idea of starting from an appropriate reference system, is that the exact solution of the latter already contains the essential correlations of the original system. These manifest themselves on the one-particle level (g) but especially also on the two-particle level. Recent studies have illustrated the value of the information encoded in vertices and susceptibilities^{22,50–58} even in the case of a single-orbital model.

In the present case, we use the critical plaquette as the reference model. This plaquette has a sixfold degenerate ground state and anomalies related to transitions between these ground states manifest themselves in the two-particle correlation functions at finite temperature through the T^{-3} behavior compared to the usual T^{-1} one in the general case.

The Bethe–Salpeter equation has an intertwined spin, site and frequency structure which can be simplified by looking at the different channels. Since our main interest is superconductivity, we consider the singlet particle-particle channel. For comparison

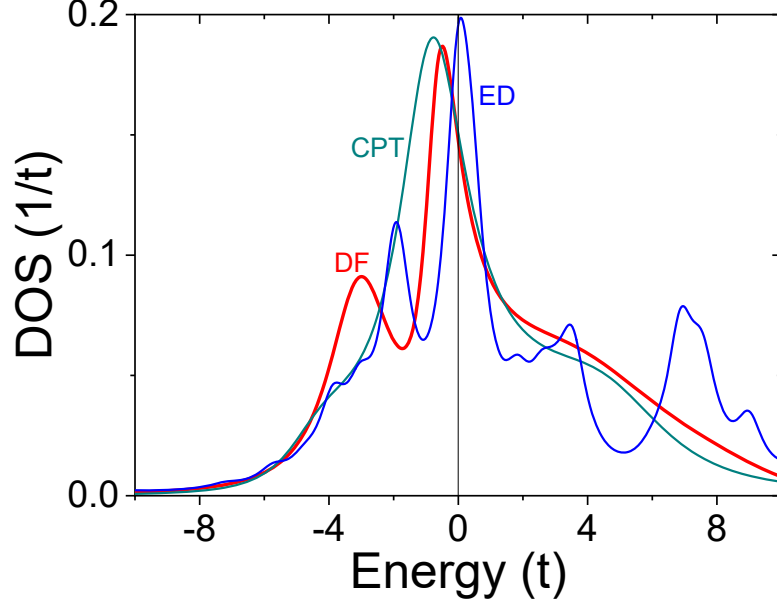


FIG. 4. Density of states for dual fermion plaquette second order scheme (DF) in comparison with the cluster perturbation theory (CPT) and exact diagonalization (ED) of 2×2 plaquette for $U = 5.56$, $t'_0 = t' = 0.15$, $\mu_0 = 0.48$ and $\mu = 1.55$, $\beta=3$.

we consider also particle-hole density and magnetic channels. Regarding the frequencies, we restrict ourselves to the lowest 10 Matsubara frequencies, since the vertex function Eq.(12) decays strongly with $(\nu, \nu')^{59}$.

Within the cluster dual fermion theory, the lattice instability manifests itself by $\lambda_{max} = 1$, where λ_i are eigenvalues of the following Bethe-Salpeter matrix $\Lambda_{i,j}$ in the case of the particle-particle singlet channel:

$$\Lambda_{12,34}^{P_{\nu\nu'}}(q, \omega) = \frac{T}{2N_k} \sum_{k; 3'4'} \gamma_{12,3'4'}^{P_{\nu\nu'}}(\omega) \tilde{G}_{4',4}(\omega - \nu', q - k) \tilde{G}_{3,3'}(\nu', k) \quad (24)$$

with $i = (12, \nu)$, $j = (34, \nu')$ and $q = 0$, $\omega = 0$. In this case the matrix γ^P is Hermitian (real for $\omega = 0$), while matrix Λ is not Hermitian, but the leading eigenvalues are still found to be real for all channels (we also calculate eigenvalues of corresponding Bethe-Salpeter equations in the density and magnetic particle-hole channels). It has been shown that lattice and dual two-particle quantities have the same set of poles⁶⁰. In the limit $T \rightarrow 0$, the plaquette vertex has several divergences ($\sim T^{-3}$), corresponding to degeneracies of the reference model, while the cluster Green's function has divergences ($\sim T^{-1}$) at the degenerate point. Results for the maximum eigenvalues of the Bethe-Salpeter matrix Λ at the critical point for $\omega = 0$ and $q = 0$ are presented in the Fig. 5.

The eigenvector corresponding to λ_{max} for the particle-particle singlet case has $d_{x^2-y^2}$ symmetry in the plaquette space. Exactly at the plaquette degenerate point the instability (signaled by λ crossing 1) in the density channel is very large because the $N = 2, 3, 4$ states are degenerate. We found that this density instability is not robust against change of μ_0 and as soon as we shift it towards low hole doping $\mu_0 = 0.8$ there is no density instability⁵⁹. On the other hand the singlet superconducting instability is very robust and becomes the leading one for doping lower than $\delta = 0.25$. The magnetic instability does not play any role for the doped case and becomes the leading one only in the half-filled case⁵⁹.

V. PAIRING MECHANISM IN REAL SPACE, EXACT DIAGONALIZATION OF 4×4 CLUSTER

To understand why superconductivity occurs, it is necessary to find a pairing mechanism, i.e., an attractive interaction between pairs of fermions. So far, we have studied the eigenvalues of the Bethe-Salpeter equation to identify such a superconducting instability. Here, we will gain additional insight from a complementary real-space method. We calculated the pairing energy of two holes on the 4×4 periodic cluster – which consists of 2×2 plaquettes – through the ground state energies in the different occupation sectors,

$$\Delta_{2h} = \tilde{E}_{2h} - 2\tilde{E}_{1h}, \quad (25)$$

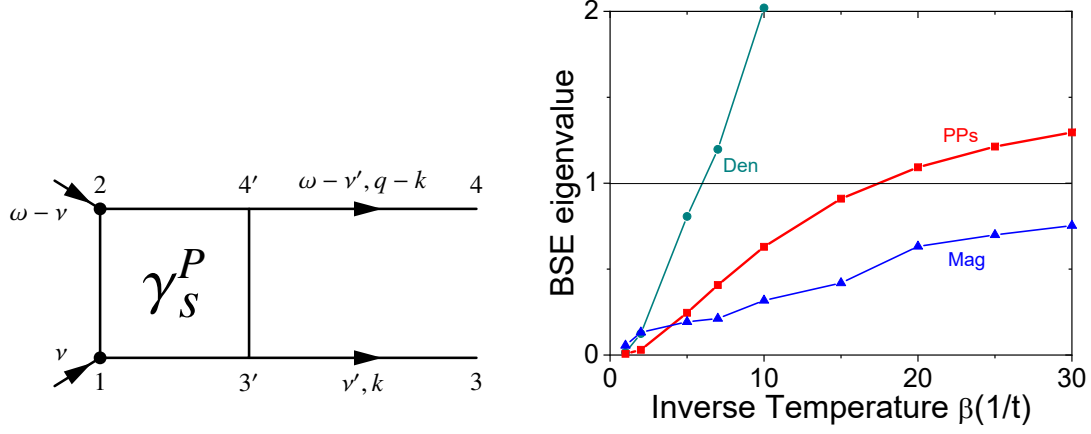


FIG. 5. Diagrammatic representation of the Bethe-Salpeter kernel in the particle-particle channel (left) and its maximum eigenvalues (right) for the particle-particle singlet (PPs), density (Den) and magnetic (Mag) channel (right) for doped plaquette with $U=5.56$ and $t'=-0.15t$, $\mu=1.55$ and

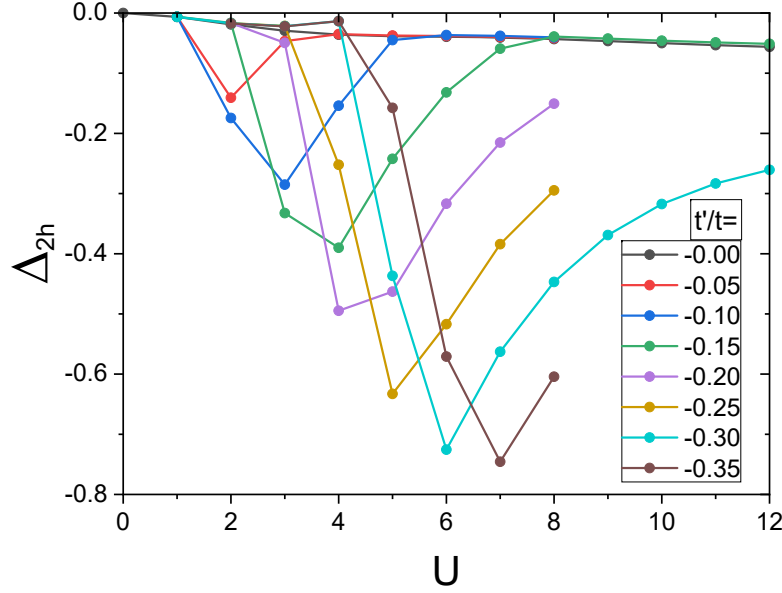


FIG. 6. Pairing energy Δ_{2h} of two holes in a 4×4 cluster with periodic boundary condition as a function of U and t' .

where the energies are measured relative to the half-filled ground states E_0 with no holes, $\tilde{E}_{Nh} = E_{Nh} - E_0$. Note, that $\Delta_{2h} < 0$ signals pairing. Calculated energies for $t' = 0$ are in the perfect agreement with the standard ED results⁶¹.

Figure 6 shows the pair binding energy Δ_{2h} between pairs of holes for a 4×4 cluster $t - t' - U$ Hubbard model with periodic boundary conditions as a function of interactions strength U for different next-nearest neighbours hopping t' . There is a very strong binding of two holes around $U = 6$ and $t'/t = -0.3$, which is consistent with the estimate for the cuprates¹⁵. The pairing energy is of the order of $\Delta_{2h}/t \approx -0.7$ which is of the order 3000 K for $t \approx 0.4$ eV for generic cuprates model^{11,15}. There is a clear change of behaviour of Δ_{2h} as a function of t' , with the vanishing of the pairing energy at small U . It can be attributed to the change of the ground state for the sector $(7\uparrow, 7\downarrow)$ at $t'/t \approx 0.12$ ⁵⁹. We also observe a drastic change of the behavior of the magnetic correlations from antiferromagnetic at $t' = 0$ to almost non-magnetic for $t'/t = -0.3$ in this sector⁵⁹. Similar energetic of hole-binding in 4×4 Hubbard cluster was found recently⁶² for a different model of inhomogeneous hopping⁶³. The effects of negative t'/t consider to be destructive for superconductivity in the $t - t' - J$ model⁶⁴. Our results (Figure 6) show that strong effect of the hole pair binding on 4×4 cluster disappear for $U \gg W = 8t$ or in $t - J$ limit.

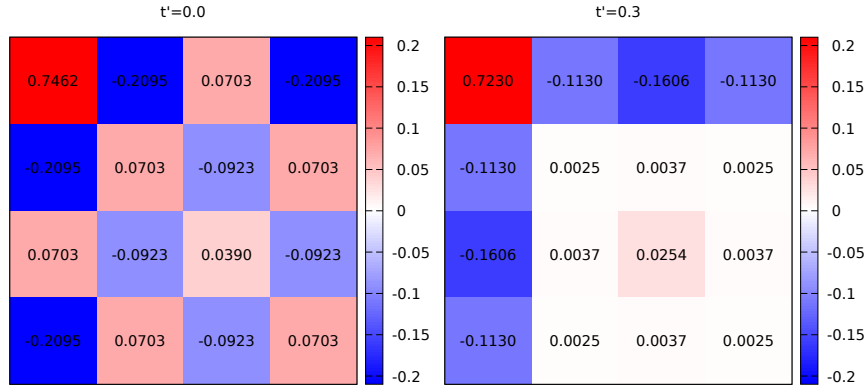


FIG. 7. Static spin-spin correlation function $\langle M_0 M_i \rangle$ obtained by exact diagonalization for the ground state of the sector $(7\uparrow, 7\downarrow)$ of the 4×4 cluster for different t' . Whereas $t' = 0$ features clear antiferromagnetic correlations, at $t'/t = -0.3$ these are replaced by stripe-like ferromagnetic correlations. The top-left corner corresponds to $i = (0, 0)$.

These results clearly show the importance of t' , which greatly increases the pairing energy gain. At the same time, in a non-interacting systems $\Delta_{2h} = 0$ by definition, so a finite value of U is also necessary for the pairing. We find that the optimal U increases with t' . A second observation is the order of magnitude of the pairing, $\Delta_{2h} \approx 0.7t \gg k_B T_c^{\text{exp}}$. This tells us that bound pairs exist for temperatures far above the superconducting region. The superconducting transition should then be seen as the condensation of these pairs. Thus, the binding energy of two holes turns out to be much higher than the superconducting critical temperature which means that the pairs (“bipolarons”) should be well-defined also in non-superconducting phase, a situation dramatically different from the conventional BCS superconductivity. The difference is like the difference between purely itinerant weak ferromagnets and ferromagnets with local magnetic moments which exist until very high temperatures and only order, rather than appear, at the Curie temperature⁶⁵.

We analyzed the spin-spin correlation function in the sector $(7\uparrow, 7\downarrow)$ with different NNN hoppings t' (Fig.7) and clearly see a sharp change from antiferromagnetic correlations for $t' = 0$ with clear “checkerboard” structure to almost nonmagnetic case or ferromagnetic stripes in the x or y directions for $t' = 0.3$. A similar reduction of AFM-correlations and existence of FM-one with t' was found in a lattice QMC study⁶⁶.

VI. SPECTRAL INFORMATION

Due to the degeneracy of states with different particle number, the density of states of the plaquette is large close to the Fermi level. The availability of low-energy states is the driving force behind the instabilities that occur once a lattice of plaquettes is considered. In Fig. 8 we compare the DOS for the plaquette DF perturbation theory for low temperature ($\beta = 5$) with the ED results for the 4×4 cluster in the sector $(7\uparrow, 7\downarrow)$, which corresponds to a 2×2 lattice of plaquettes. These two methods are complementary: the DF approach is perturbative in the inter-plaquette coupling and able to handle large lattices, whereas the ED is exact but limited by the cluster size. From the comparison of the two curves, we conclude that the dual fermion theory shows a tendency towards pseudogap formation which is clearly seen in the ED results. It is natural to conclude that the pseudogap in the 4×4 cluster is related to the coherent interactions of the large peak on the DOS in the reference plaquette or Fano-like effect of interactions with the “soft fermion mode” of the low-lying excitations which are encoded in the local vertex functions of the DF-approach. In this sense the pseudogap physics is not related to the magnetic fluctuations, and is more in line with the “hidden fermion” physics^{67,68} or “destructive interference phenomena”⁶⁹.

VII. CONCLUSIONS

The physics of cuprate superconductors with the clear existence of a quantum critical point at $\delta_c \approx 0.24$ is closely related to the degeneracy of the plaquette in the strong-coupling regime. In this sense, the plaquette and not the single site can be considered the minimal building block for cuprate physics. The renormalized dual fermion perturbation starting from the plaquette reference system with $\delta = 0.25$ uncovers consequences of this degeneracy for the Green’s function in the lattice and shows the basic “plaquette” mechanism of superconducting instability in the Bethe-Salpeter equation for a general cuprate model. Exact diagonalization of the 4×4 cluster supports strong pair-binding related with the next-nearest hoppings t' . Given their large binding energy, these pairs should probably exist also at much higher temperatures than the superconducting critical temperature, remaining noncoherent. The formation of the pseudogap is related to a Fano-like effect originating from the sharply peaked

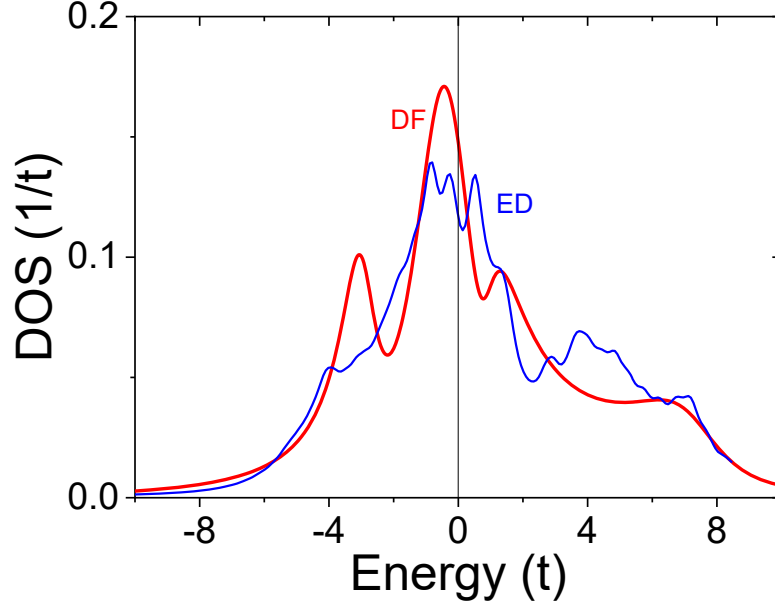


FIG. 8. Density of states for dual fermion plaquette perturbation (DF) with $\beta = 5$ in comparison with exact diagonalisation (ED) for 4×4 periodic cluster. See Fig. 4 for other parameters.

DOS in the isolated plaquette embedded into the band of surrounding fermions, as was hypothesised in Ref.¹⁶. In the overdoped regime $\delta \geq 0.25$ the strong charge fluctuations restore formation of the normal metallic phase and corresponding Bethe-Salpeter equation does not indicate any instabilities. For the doping $\delta \leq 0.25$ the dual perturbation theory starting from the plaquette clearly shows a low temperature $d_{x^2-y^2}$ instability. These observations can all be made by starting the perturbation theory from an isolated plaquette. For more quantitative predictions of the theoretical phase diagram, the optimal dynamical embedding of the plaquette and the implications for the resulting perturbation theory need to be studied further.

ACKNOWLEDGMENTS

The authors thank Alexei Rubtsov, Evgeny Stepanov, Igor Krivenko, Fedor Šimkovic IV, Georg Rohringer, Andy Millis and Antoine Georges for valuable comments on the work. E.G.C.P.v.L. is supported by the Zentrale Forschungsförderung of the Universität Bremen. This work was partially supported by the Cluster of Excellence “Advanced Imaging of Matter” of the Deutsche Forschungsgemeinschaft (DFG) - EXC 2056 - Project No. ID390715994, by European Research Council via Synergy Grant 854843 - FASTCORR and by North-German Supercomputing Alliance (HLRN) under the Project No. hhp00042.

* erik.van_loon@teorfys.lu.se

† alichten@physnet.uni-hamburg.de

¹ J. G. Bednorz and K. A. Müller, “Possible high Tc superconductivity in the BaLaCuO system,” *Zeitschrift für Physik B Condensed Matter* **64**, 189–193 (1986).

² Xingjiang Zhou, Wei-Sheng Lee, Masatoshi Imada, Nandini Trivedi, Philip Phillips, Hae-Young Kee, Päivi Törmä, and Mikhail Erements, “High-temperature superconductivity,” *Nature Reviews Physics* **3**, 462–465 (2021).

³ D. J. Scalapino, “A common thread: The pairing interaction for unconventional superconductors,” *Rev. Mod. Phys.* **84**, 1383–1417 (2012).

⁴ I. Esterlis, S. A. Kivelson, and D. J. Scalapino, “A bound on the superconducting transition temperature,” *npj Quantum Materials* **3**, 59 (2018).

⁵ B. Keimer, S. A. Kivelson, M. R. Norman, S. Uchida, and J. Zaanen, “From quantum matter to high-temperature superconductivity in copper oxides,” *Nature* **518**, 179–186 (2015).

⁶ Hong-Chen Jiang and Thomas P. Devereaux, “Superconductivity in the doped hubbard model and its interplay with next-nearest hopping t' ,” *Science* **365**, 1424–1428 (2019), <https://science.sciencemag.org/content/365/6460/1424.full.pdf>.

- ⁷ Mingpu Qin, Chia-Min Chung, Hao Shi, Ettore Vitali, Claudius Hubig, Ulrich Schollwöck, Steven R. White, and Shiwei Zhang (Simons Collaboration on the Many-Electron Problem), “Absence of superconductivity in the pure two-dimensional Hubbard model,” *Phys. Rev. X* **10**, 031016 (2020).
- ⁸ Cyril Proust and Louis Taillefer, “The remarkable underlying ground states of cuprate superconductors,” *Annual Review of Condensed Matter Physics* **10**, 409–429 (2019), <https://doi.org/10.1146/annurev-conmatphys-031218-013210>.
- ⁹ J. Ayres, M. Berben, M. Culo, Y. T. Hsu, E. van Heumen, Y. Huang, J. Zaanen, T. Kondo, T. Takeuchi, J. R. Cooper, C. Putzke, S. Friedemann, A. Carrington, and N. E. Hussey, “Incoherent transport across the strange metal regime of highly overdoped cuprates,” *Nature* (2021), arXiv:2012.01208 [cond-mat.str-el].
- ¹⁰ M. Culo, C. Duffy, J. Ayres, M. Berben, Y.-T. Hsu, R. D. H. Hinlopen, B. Bernath, and N. E. Hussey, “Possible superconductivity from incoherent carriers in overdoped cuprates,” *SciPost Phys.* **11**, 12 (2021).
- ¹¹ O. K. Andersen, O. Jepsen, A. I. Liechtenstein, and I. I. Mazin, “Plane dimpling and saddle-point bifurcation in the band structures of optimally doped high-temperature superconductors: A tight-binding model,” *Phys. Rev. B* **49**, 4145–4157 (1994).
- ¹² C. Collignon, S. Badoux, S. A. A. Afshar, B. Michon, F. Laliberté, O. Cyr-Choinière, J.-S. Zhou, S. Licciardello, S. Wiedmann, N. Doiron-Leyraud, and Louis Taillefer, “Fermi-surface transformation across the pseudogap critical point of the cuprate superconductor $\text{La}_{1.6-x}\text{Nd}_{0.4}\text{Sr}_x\text{CuO}_4$,” *Phys. Rev. B* **95**, 224517 (2017).
- ¹³ G. Rohringer, H. Hafermann, A. Toschi, A. A. Katanin, A. E. Antipov, M. I. Katsnelson, A. I. Lichtenstein, A. N. Rubtsov, and K. Held, “Diagrammatic routes to nonlocal correlations beyond dynamical mean field theory,” *Rev. Mod. Phys.* **90**, 025003 (2018).
- ¹⁴ H. Hafermann, S. Brener, A. N. Rubtsov, M. I. Katsnelson, and A. I. Lichtenstein, “Cluster dual fermion approach to nonlocal correlations,” *JETP Letters* **86**, 677–682 (2008).
- ¹⁵ E. Pavarini, I. Dasgupta, T. Saha-Dasgupta, O. Jepsen, and O. K. Andersen, “Band-structure trend in hole-doped cuprates and correlation with t_{cmax} ,” *Phys. Rev. Lett.* **87**, 047003 (2001).
- ¹⁶ Malte Harland, Mikhail I. Katsnelson, and Alexander I. Lichtenstein, “Plaquette valence bond theory of high-temperature superconductivity,” *Phys. Rev. B* **94**, 125133 (2016).
- ¹⁷ A. I. Lichtenstein and M. I. Katsnelson, “Antiferromagnetism and d-wave superconductivity in cuprates: A cluster dynamical mean-field theory,” *Phys. Rev. B* **62**, R9283–R9286 (2000).
- ¹⁸ Ehud Altman and Assa Auerbach, “Plaquette boson-fermion model of cuprates,” *Phys. Rev. B* **65**, 104508 (2002).
- ¹⁹ Alexander Cyril Hewson, *The Kondo Problem to Heavy Fermions* (Cambridge University Press, Cambridge, 1993).
- ²⁰ I. S. Krivenko, A. N. Rubtsov, M. I. Katsnelson, and A. I. Lichtenstein, “Analytical approximation for single-impurity anderson model,” *JETP Letters* **91**, 319–325 (2010).
- ²¹ Wei Wu, Michel Ferrero, Antoine Georges, and Evgeny Kozik, “Controlling feynman diagrammatic expansions: Physical nature of the pseudogap in the two-dimensional hubbard model,” *Phys. Rev. B* **96**, 041105 (2017).
- ²² Malte Harland, Sergey Brener, Mikhail I. Katsnelson, and Alexander I. Lichtenstein, “Exactly solvable model of strongly correlated d -wave superconductivity,” *Phys. Rev. B* **101**, 045119 (2020).
- ²³ A. N. Rubtsov, M. I. Katsnelson, and A. I. Lichtenstein, “Dual fermion approach to nonlocal correlations in the hubbard model,” *Phys. Rev. B* **77**, 033101 (2008).
- ²⁴ Sergey Brener, Evgeny A. Stepanov, Alexey N. Rubtsov, Mikhail I. Katsnelson, and Alexander I. Lichtenstein, “Dual fermion method as a prototype of generic reference-system approach for correlated fermions,” *Annals of Physics* **422**, 168310 (2020).
- ²⁵ Andrey A. Bagrov, Mikhail Danilov, Sergey Brener, Malte Harland, Alexander I. Lichtenstein, and Mikhail I. Katsnelson, “Detecting quantum critical points in the $t - t'$ Fermi-Hubbard model via complex network theory,” *Scientific Reports* **10**, 20470 (2020).
- ²⁶ Hartmut Hafermann, Frank Lechermann, Alexey N. Rubtsov, Mikhail I. Katsnelson, Antoine Georges, and Alexander I. Lichtenstein, “Strong electronic correlations: Dynamical mean-field theory and beyond,” in *Modern theories of many-particle systems in condensed matter physics*, Vol. 843, edited by Daniel C Cabra, Andreas Honecker, and Pierre Pujol (Springer Science & Business Media, 2012) Chap. 4.
- ²⁷ Nayuta Takemori, Akihisa Koga, and Hartmut Hafermann, “Intersite electron correlations on inhomogeneous lattices: a real-space dual fermion approach,” (2018), arXiv:1801.02441 [cond-mat.str-el].
- ²⁸ Emanuel Gull, Andrew J. Millis, Alexander I. Lichtenstein, Alexey N. Rubtsov, Matthias Troyer, and Philipp Werner, “Continuous-time monte carlo methods for quantum impurity models,” *Rev. Mod. Phys.* **83**, 349–404 (2011).
- ²⁹ R. L. Stratonovich, “On a method of calculating quantum distribution functions,” in *Soviet Physics Doklady*, Vol. 2 (1957) p. 416.
- ³⁰ J. Hubbard, “Calculation of partition functions,” *Phys. Rev. Lett.* **3**, 77–78 (1959).
- ³¹ Erik G C P van Loon, “Second-order dual fermion for multi-orbital systems,” *Journal of Physics: Condensed Matter* **33**, 135601 (2021).
- ³² S K Sarker, “A new functional integral formalism for strongly correlated fermi systems,” *Journal of Physics C: Solid State Physics* **21**, L667–L672 (1988).
- ³³ Stéphane Pairault, David Sénéchal, and A.-M. S. Tremblay, “Strong-coupling expansion for the Hubbard model,” *Phys. Rev. Lett.* **80**, 5389–5392 (1998).
- ³⁴ Pairault, S., Sénéchal, D., and A.-M.S. Tremblay, “Strong-coupling perturbation theory of the Hubbard model,” *Eur. Phys. J. B* **16**, 85–105 (2000).
- ³⁵ N. Dupuis and S. Pairault, “A strong-coupling expansion for the Hubbard model,” *International Journal of Modern Physics B* **14**, 2529–2560 (2000), <https://doi.org/10.1142/S0217979200002430>.
- ³⁶ N. Dupuis, “A new approach to strongly correlated fermion systems: the spin–particle–hole coherent-state path integral,” *Nuclear Physics B* **618**, 617 – 649 (2001).
- ³⁷ Claudius Gros and Roser Valentí, “Cluster expansion for the self-energy: A simple many-body method for interpreting the photoemission spectra of correlated fermi systems,” *Phys. Rev. B* **48**, 418–425 (1993).
- ³⁸ H. Hafermann, *Numerical Approaches to Spatial Correlations in Strongly Interacting Fermion Systems*, Ph.D. thesis, Universität Hamburg (2009).

- ³⁹ H. Hafermann, G. Li, A. N. Rubtsov, M. I. Katsnelson, A. I. Lichtenstein, and H. Monien, “Efficient perturbation theory for quantum lattice models,” *Phys. Rev. Lett.* **102**, 206401 (2009).
- ⁴⁰ Friedrich Krien, Angelo Valli, Patrick Chalupa, Massimo Capone, Alexander I. Lichtenstein, and Alessandro Toschi, “Boson-exchange parquet solver for dual fermions,” *Phys. Rev. B* **102**, 195131 (2020).
- ⁴¹ Sergei Isakov, Andrey E. Antipov, and Emanuel Gull, “Diagrammatic monte carlo for dual fermions,” *Phys. Rev. B* **94**, 035102 (2016).
- ⁴² Jan Gukelberger, Evgeny Kozik, and Hartmut Hafermann, “Diagrammatic monte carlo approach for diagrammatic extensions of dynamical mean-field theory: Convergence analysis of the dual fermion technique,” *Phys. Rev. B* **96**, 035152 (2017).
- ⁴³ M. Vandelli, V. Harkov, E. A. Stepanov, J. Gukelberger, E. Kozik, A. Rubio, and A. I. Lichtenstein, “Dual boson diagrammatic monte carlo approach applied to the extended hubbard model,” *Phys. Rev. B* **102**, 195109 (2020).
- ⁴⁴ E.G.C.P. van Loon, “dualfermion,” <https://github.com/egcpvanloon/dualfermion/> (2020).
- ⁴⁵ Olivier Parcollet, Michel Ferrero, Thomas Ayrat, Hartmut Hafermann, Igor Krivenko, Laura Messio, and Priyanka Seth, “Triqs: A toolbox for research on interacting quantum systems,” *Computer Physics Communications* **196**, 398 – 415 (2015).
- ⁴⁶ Andrey E. Antipov, Igor Krivenko, and Sergei Isakov, “aeantipov/pomerol: 1.2,” (2017).
- ⁴⁷ Sergei Isakov, Hanna Terletska, and Emanuel Gull, “Momentum-space cluster dual-fermion method,” *Phys. Rev. B* **97**, 125114 (2018).
- ⁴⁸ H. Hafermann, C. Jung, S. Brener, M. I. Katsnelson, A. N. Rubtsov, and A. I. Lichtenstein, “Superperturbation solver for quantum impurity models,” *EPL (Europhysics Letters)* **85**, 27007 (2009).
- ⁴⁹ Antoine Georges, Gabriel Kotliar, Werner Krauth, and Marcelo J. Rozenberg, “Dynamical mean-field theory of strongly correlated fermion systems and the limit of infinite dimensions,” *Rev. Mod. Phys.* **68**, 13–125 (1996).
- ⁵⁰ G. Rohringer, A. Valli, and A. Toschi, “Local electronic correlation at the two-particle level,” *Phys. Rev. B* **86**, 125114 (2012).
- ⁵¹ T. Schäfer, G. Rohringer, O. Gunnarsson, S. Ciuchi, G. Sangiovanni, and A. Toschi, “Divergent precursors of the Mott-Hubbard transition at the two-particle level,” *Phys. Rev. Lett.* **110**, 246405 (2013).
- ⁵² Evgeny Kozik, Michel Ferrero, and Antoine Georges, “Nonexistence of the Luttinger-Ward functional and misleading convergence of skeleton diagrammatic series for Hubbard-like models,” *Phys. Rev. Lett.* **114**, 156402 (2015).
- ⁵³ Friedrich Krien, Erik G. C. P. van Loon, Mikhail I. Katsnelson, Alexander I. Lichtenstein, and Massimo Capone, “Two-particle fermi liquid parameters at the mott transition: Vertex divergences, landau parameters, and incoherent response in dynamical mean-field theory,” *Phys. Rev. B* **99**, 245128 (2019).
- ⁵⁴ D. Springer, P. Chalupa, S. Ciuchi, G. Sangiovanni, and A. Toschi, “Interplay between local response and vertex divergences in many-fermion systems with on-site attraction,” *Phys. Rev. B* **101**, 155148 (2020).
- ⁵⁵ Corey Melnick and Gabriel Kotliar, “Fermi-liquid theory and divergences of the two-particle irreducible vertex in the periodic anderson lattice,” *Phys. Rev. B* **101**, 165105 (2020).
- ⁵⁶ Erik G. C. P. van Loon, Friedrich Krien, and Andrey A. Katanin, “Bethe-salpeter equation at the critical end point of the mott transition,” *Phys. Rev. Lett.* **125**, 136402 (2020).
- ⁵⁷ M. Reitner, P. Chalupa, L. Del Re, D. Springer, S. Ciuchi, G. Sangiovanni, and A. Toschi, “Attractive effect of a strong electronic repulsion: The physics of vertex divergences,” *Phys. Rev. Lett.* **125**, 196403 (2020).
- ⁵⁸ P. Chalupa, T. Schäfer, M. Reitner, D. Springer, S. Andergassen, and A. Toschi, “Fingerprints of the local moment formation and its kondo screening in the generalized susceptibilities of many-electron problems,” *Phys. Rev. Lett.* **126**, 056403 (2021).
- ⁵⁹ Michael Danilov et. al., “Supplemental materials,” (2021).
- ⁶⁰ S. Brener, H. Hafermann, A. N. Rubtsov, M. I. Katsnelson, and A. I. Lichtenstein, “Dual fermion approach to susceptibility of correlated lattice fermions,” *Phys. Rev. B* **77**, 195105 (2008).
- ⁶¹ E. Dagotto, A. Moreo, F. Ortolani, D. Poilblanc, and J. Riera, “Static and dynamical properties of doped hubbard clusters,” *Phys. Rev. B* **45**, 10741–10760 (1992).
- ⁶² Gideon Wachtel, Shirit Baruch, and Dror Orgad, “Optimal inhomogeneity for pairing in hubbard systems with next-nearest-neighbor hopping,” *Phys. Rev. B* **96**, 064527 (2017).
- ⁶³ Wei-Feng Tsai, Hong Yao, Andreas Läuchli, and Steven A. Kivelson, “Optimal inhomogeneity for superconductivity: Finite-size studies,” *Phys. Rev. B* **77**, 214502 (2008).
- ⁶⁴ G. B. Martins, J. C. Xavier, L. Arrachea, and E. Dagotto, “Qualitative understanding of the sign of t' asymmetry in the extended $t-j$ model and relevance for pairing properties,” *Phys. Rev. B* **64**, 180513 (2001).
- ⁶⁵ Toru Moriya, *Spin Fluctuations in Itinerant Electron Magnetism* (Springer Verlag, New York, 1985).
- ⁶⁶ Shuhui Yang, Tao Ying, Weiqi Li, Jianqun Yang, Xiudong Sun, and Xingji Li, “Quantum monte carlo study of the hubbard model with next-nearest-neighbor hopping t' : pairing and magnetism,” *Journal of Physics: Condensed Matter* **33**, 115601 (2020).
- ⁶⁷ Shiro Sakai, Marcello Civelli, and Masatoshi Imada, “Hidden fermionic excitation boosting high-temperature superconductivity in cuprates,” *Phys. Rev. Lett.* **116**, 057003 (2016).
- ⁶⁸ Shiro Sakai, Marcello Civelli, and Masatoshi Imada, “Hidden-fermion representation of self-energy in pseudogap and superconducting states of the two-dimensional hubbard model,” *Phys. Rev. B* **94**, 115130 (2016).
- ⁶⁹ J. Merino and O. Gunnarsson, “Pseudogap and singlet formation in organic and cuprate superconductors,” *Phys. Rev. B* **89**, 245130 (2014).
- ⁷⁰ D. Rost, E. V. Gorelik, F. Assaad, and N. Blümer, “Momentum-dependent pseudogaps in the half-filled two-dimensional hubbard model,” *Phys. Rev. B* **86**, 155109 (2012).
- ⁷¹ Elbio Dagotto, Robert Joynt, Adriana Moreo, Silvia Bacci, and Eduardo Gagliano, “Strongly correlated electronic systems with one hole: Dynamical properties,” *Phys. Rev. B* **41**, 9049–9073 (1990).

Appendix A: Exact relations for Green's function

After appropriate diagrammatic results for the dual self-energy and the dual Green function has been obtained, it has to be transformed back to the corresponding physical quantities in terms of real lattice fermions. The fact that dual fermions are introduced through the exact Hubbard-Stratonovich transformation Eq. (5) allows to establish exact identities between dual and lattice Greens function^{23,38}.

The relations between the n -particle cumulants of the dual and lattice fermions can be established using the cumulant (linked cluster) technique. To this end, one may consider two different, equivalent representations of the following generating functional:

$$e^{-F[J^*, J, L^*, L]} = \int \mathcal{D}[c^*, c, d^*, d] e^{-S[c^*, c, d^*, d] + J_1^* c_1 + c_2^* J_2 + L_1^* d_1 + d_2^* L_2} \quad (\text{A1})$$

Integrating out the lattice fermions from this functional similar to (9) (this can be done with the sources J and J^* set to zero) yields

$$e^{-F[L^*, L]} = \int \mathcal{D}[d^*, d] e^{-\tilde{S}[d^*, d] + L_1^* d_1 + d_2^* L_2} \quad (\text{A2})$$

The dual Green function and the two-particle correlator related to the non-local susceptibilities are obtained from (A2) by suitable functional derivatives, e.g.

$$\tilde{G}_{12} = \left. \frac{\delta^2 F}{\delta L_2 \delta L_1^*} \right|_{L^*=L=0} \quad (\text{A3})$$

Integrating out the dual fermions from Eq.(A1) using the HST, one obtains an alternative representation, which more clearly reveals a connection of the functional derivatives with respect to the sources J, J^* and L, L^* . The result is

$$F[J^*, J, L^*, L] = L_1^* (t - \Delta)_{12} L_2 - \ln \int \mathcal{D}[c^*, c] \exp \left(-S[c^*, c] + J_1^* c_1 + c_2^* J_2 - L_1^* (t - \Delta)_{12} c_2 - c_1^* (t - \Delta)_{12} L_2 \right). \quad (\text{A4})$$

In analogy to (A3), the cumulants in terms of lattice fermions are obviously obtained by functional derivative with respect to the sources J and J^* with L and L^* set to zero. Applying the derivatives with respect to L, L^* to (A4) with $J = J^* = 0$ and comparing to (A3), e.g. yields the following identity:

$$G_{12} = -(t - \Delta)_{12}^{-1} + (t - \Delta)_{11'}^{-1} \tilde{G}_{1'2'} (t - \Delta)_{2'2}^{-1}. \quad (\text{A5})$$

Appendix B: Plaquette periodization

By breaking up the original lattice into plaquettes, the translational symmetry is broken: bonds within a plaquette are treated differently from bonds between plaquettes. We need to restore the full translational symmetry and then all quantities can be written in terms of the momentum \mathbf{k} in the Brillouin Zone of the original lattice.

Let us discuss a periodization of plaquette self-energy $\Sigma_{ij}(\mathbf{r}, \nu)$ Eq. (17) where $\mathbf{r} \equiv (r_x, r_y)$ is the supercell translation and i, j are cluster sites (see Fig.(9)). The latter can be alternatively described by intra-plaquette translation vectors \mathbf{i}, \mathbf{j} taking values $[(0, 0), (0, 1), (1, 1), (1, 0)]$ for the site indices 0 to 3 respectively. We would like to get a lattice periodic self-energy $\Sigma(\mathbf{R}, \nu)$ where $\mathbf{R} \equiv (R_x, R_y)$ is the original square lattice translations. By construction Σ is periodic in \mathbf{r} , but not in \mathbf{R} . The natural periodization procedure would be taking all four possible values of $\mathbf{i} \equiv (i_x, i_y)$ and average over them for a given value of \mathbf{R} . This is done straightforwardly with a minor technical challenge of determining the supercell translation \mathbf{r} and final site index \mathbf{j} that correspond to a given value of lattice translation \mathbf{R} and initial site index \mathbf{i} . By recasting

$$\mathbf{i} + \mathbf{R} \equiv (i_x + R_x, i_y + R_y) = (2[(i_x + R_x)/2] + 2\{(i_x + R_x)/2\}, 2[(i_y + R_y)/2] + 2\{(i_y + R_y)/2\}), \quad (\text{B1})$$

and noticing that $\mathbf{i} + \mathbf{R} = \mathbf{j} + 2\mathbf{r}$, we immediately find $\mathbf{r}(\mathbf{i}, \mathbf{R}) = ([(i_x + R_x)/2], [(i_y + R_y)/2])$ and $\mathbf{j}(\mathbf{i}, \mathbf{R}) = (2\{(i_x + R_x)/2\}, 2\{(i_y + R_y)/2\})$. Here $[x]$ and $\{x\}$ are the integer and fractional parts of x respectively. Finally we take for the periodized self-energy:

$$\Sigma(\mathbf{R}, \nu) = \frac{1}{4} \sum_{\mathbf{i}} \Sigma_{ij}(\mathbf{i}, \mathbf{R})(\mathbf{r}(\mathbf{i}, \mathbf{R}), \nu), \quad (\text{B2})$$

with the sum being taken over four cluster sites.

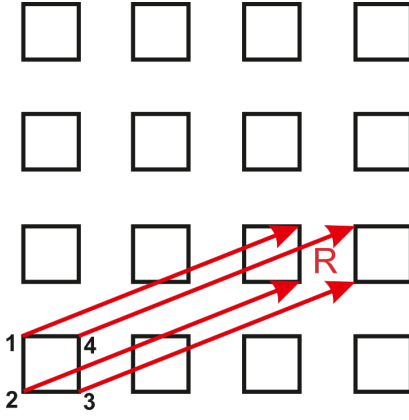


FIG. 9. Scheme for the real-space periodization of the 2×2 plaquette lattice.

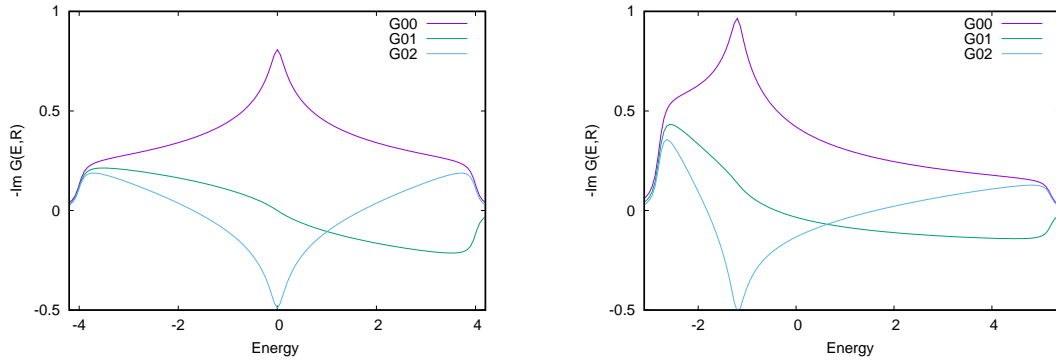


FIG. 10. Plaquette supercell Green's function $-\text{Im } G(E, r)$ for $U = 0$, $t'/t = 0$ (left) and $t'/t = -0.3$ (right) with $r = (0, 0)$, $r = (0, 1)$ and $r = (1, 1)$.

Appendix C: The non-interacting system

At $U = 0$, the Hubbard model becomes a tight-binding model that is diagonalized by going to the momentum basis. Figure 10 presents the resulting bare Green's function. The local part (G_{11} , only the imaginary part is shown) is related to the local DOS and displays the familiar Van Hove singularity at $E = 0$ for $t' = 0$. For $t'/t = -0.3$, the Van Hove singularity shifts down to $E = -1.2 = 4t'$, and becomes more extended. More interesting is that the next-nearest-neighbor part G_{13} (again, we show the imaginary part) is also very large in magnitude and close to the Van Hove singularity it has the same order of magnitude as the local part. The next-nearest-neighbor part corresponds to the same displacement as the hopping parameter t' .

In the DF perturbation theory based on the plaquette, we calculate the self-energy corrections to this bare Green's function and we find that this self-energy effectively increases t' and makes the extended Van Hove bands almost flat with large density of states near the Fermi level. This boosts the tendency towards instabilities such as superconductivity.

In CDMFT, it is necessary to perform CT-QMC calculations to solve the impurity problem, which is computationally expensive and always introduces (substantial) numerical uncertainty. Furthermore, hybridization with the bath will wash out the degenerate point of the plaquette. Since we believe that the degenerate point contains the essential physical ingredients for the cuprate problem, here we decided to use the plaquette at the degenerate point as the dual fermion reference model for all calculations and discuss the related fluctuations and instabilities.

Appendix D: Dual perturbation theory at half-filling

We also did calculations for the half-filled square lattice Hubbard model and compared the dual fermion self-energy with the doped case. The parameters were chosen as following: $t = 1$, $t' = 0$, $U = 8$ (equal to the bandwidth $W = 8t$) and

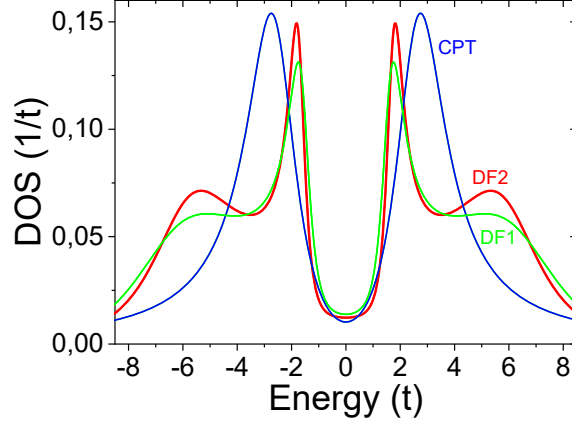


FIG. 11. Density of states for the half-filled case with $t' = 0$ and $U = W = 8$ in the zeroth-order DF approximation (CPT), the first-order (DF1) and the second order DF-theory (DF2)

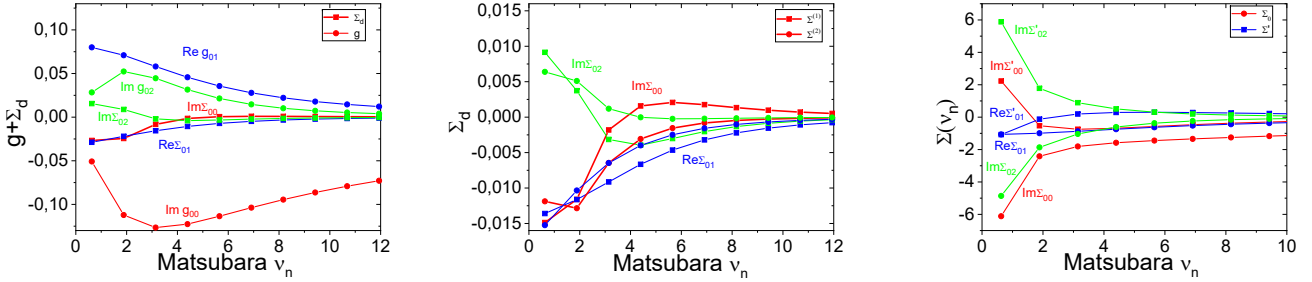


FIG. 12. Green's function of the half-filled reference plaquette (g) and local plaquette part of the dual self-energy ($\tilde{\Sigma}$) of the second order DF perturbation (left). Dual self-energy for the 1-st ($\tilde{\Sigma}^{(1)}$) and 2-nd ($\tilde{\Sigma}^{(2)}$) order DF perturbation (middle). Self-energy for the reference system and the non-local DF part (Σ') (right)

the temperature $\beta = 5$. Similar calculations have previously been done for higher temperature²⁴. The density of states for the different approximations is presented in Fig. 11. The zeroth order dual approximation ($\tilde{\Sigma} = 0$) corresponds to the cluster perturbation theory³⁷, where only the cluster self-energy was taken into account in the lattice model. The DOS for the first- and second order dual fermion plaquette perturbations are quite similar and are very different from the CPT approximation. The DF theory reproduces the so-called four-peak structure of the half-filled Hubbard model, which is also obtained in lattice QMC calculations⁷⁰.

Let us discuss, how such a strong renormalization can be seen in the dual-self energy. We start from the definition of the lattice Green's function in the dual fermion theory in Eq. (18), where the calculated self-energy enters in the following combination $(g_v + \tilde{\Sigma}_{kv})$, which shows that $\tilde{\Sigma}$ has the meaning of a T-matrix-like quantity which adds to the “bare” plaquette Green's function g . Therefore we show these two summands in Fig. 12, as a function of the Matsubara frequency. We show only the plaquette-local (*i.e.* summed over \mathbf{k} but keeping the plaquette site indices) part of the dual self-energy. We use the anticlockwise numbering of plaquette sites from 0 to 3, similar to Fig. 9. There are only three non-equivalent elements of the plaquette-local self-energy: the diagonal part $\tilde{\Sigma}_{00}$, nearest neighbour (along hopping t) $\tilde{\Sigma}_{01}$ and next-nearest neighbour (along hopping t') $\tilde{\Sigma}_{02}$. The same holds for the plaquette Green's function g_{ij} . Moreover, due to the particle-hole symmetry for the half-filled case with $t' = 0$ the only non-zero elements of these complex functions in Matsubara space are the imaginary parts of $\tilde{\Sigma}_{00}$ and $\tilde{\Sigma}_{02}$ and the real part of $\tilde{\Sigma}_{01}$. One can see from the left panel of Fig. (12) that $\text{Im } \tilde{\Sigma}_{00}$ effectively makes $\text{Im } g_{00}$ less insulating, *i.e.*, it reduces the gap. There is also an appreciable reduction of $\text{Re } g_{01}$ due to the opposite sign of $\text{Re } \tilde{\Sigma}_{01}$, which corresponds to the effective reduction of the nearest-neighbour hopping t due to correlation effects. The effect of $\text{Im } \tilde{\Sigma}_{02}$ is quite small compared to $\text{Im } g_{02}$.

In the middle panel of the Fig. 12 we show separate contributions to the dual self-energy from the first-order diagram, Eq. (20), labelled with dots and a plaquette-local part of the second-order diagram, Eq. 21, labelled with squares. Both contributions are of the same order and have the same sign, which is quite different from the doped case where we observed a significant cancellation effect by the second-order contributions.

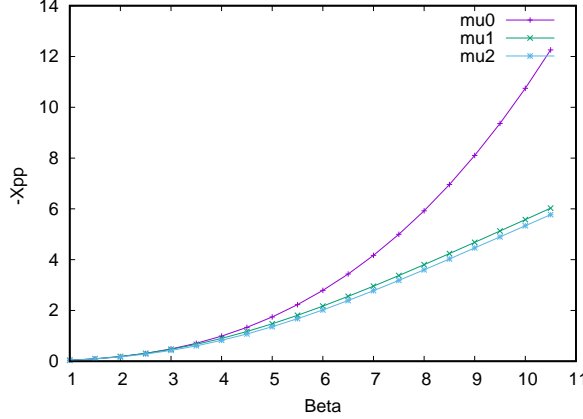


FIG. 13. The main non-local component of particle-particle generalized susceptibility χ_{0110} for plaquette with optimal parameters for degenerate point $\mu_0 = 0.48$ (mu0) and shifted $\mu_1 = 0.8$ (mu1) and $\mu_2 = 0.0$ (mu2) as function of inverse temperature β .

We can also transform self-energies back to the real fermionic representations and compare the plaquette self-energy Σ_0 with the plaquette-local part of the additional DF-contribution Σ' (Fig. 12, right panel). There is strong compensation of the local part $\text{Im } \Sigma_{00}$ as well as the second-neighbour part $\text{Im } \Sigma_{02}$, while the nearest-neighbour self-energies $\text{Re } \Sigma_{01}$ are small and have the same sign.

Appendix E: Plaquette generalized susceptibility and the degenerate point

For all DF-calculations we used 44 fermionic Matsubara frequencies for the dual Green's function and for the vertex we used 22/21 fermion/boson frequencies. We checked few calculations with up to 160 Matsubara frequencies and results are not very sensitive and well converged due to fast decay of the four point correlation functions for $\beta \leq 10$.

The generalized susceptibility $\chi_{ijkl}^P(\nu, \nu', \omega)$ is an important quantity that describes the two-particle correlations in a given channel. For the particle-particle case it merely coincides with the two-particle Green's function $\kappa_{ijkl}^P(\nu, \nu', \omega)$, while in the particle-hole channel χ differs from κ by the disconnected contribution $g_{ij}(\nu)g_{kl}(\nu')\delta_{\omega,0}$. In this appendix ω will be set to 0 everywhere and we omit it in the notation.

Let us look at the structure of the particle-particle generalized susceptibility in more detail. We define the superconducting nonlocal pairing operator as $\Delta_{ij}(\nu) = c_{i,\nu}^\dagger c_{j,-\nu}^\dagger$ (in order not to overload the formulas we consider only the $\omega = 0$ situation). The singlet pairing corresponds to $(\uparrow\downarrow - \downarrow\uparrow)/\sqrt{2}$ combination, or equivalently the singlet pairing operator is given by $\Delta_{ij}^s(\nu) = (\Delta_{ij}(\nu) + \Delta_{ji}(-\nu))/\sqrt{2}$. The generalized particle-particle singlet susceptibility is defined as

$$\chi_{ijkl}^s(\nu, \nu') = \langle \Delta_{ij}^s(\nu) \Delta_{kl}^{s\dagger}(\nu') \rangle = \chi_{ijkl}^{P\uparrow\downarrow\uparrow\downarrow}(\nu, \nu') - \chi_{ijkl}^{P\uparrow\downarrow\downarrow\uparrow}(\nu, \nu') = \chi_{ijkl}^{P\uparrow\downarrow\uparrow\downarrow}(\nu, \nu') + \chi_{ijlk}^{P\uparrow\downarrow\uparrow\downarrow}(\nu, -\nu') \quad (\text{E1})$$

To understand the special role of the plaquette degenerate point, we consider a single component of the particle-particle singlet susceptibility of the plaquette, namely χ_{0110}^s at $\nu = \nu' = \pi/\beta$. Figure 13 shows this object as a function of the inverse temperature for three different chemical potentials μ_i . At high temperature, the three different chemical potentials give essentially the same result, since $\Delta\mu \times \beta \ll 1$. However, at low temperature, we find both quantitative and qualitative changes. The degenerate point corresponds to $\mu_0 \approx 0.48$ and at low temperature we find the scaling $-\chi_{0110} \sim \beta^3$. For slightly shifted chemical potential: $\mu_1 = 0.8$ and $\mu_2 = 0.0$ (see Fig.1) we obtain the standard linear behaviour as a function of β . We conclude that the degeneracy strongly enhances the corresponding components of the susceptibility at low temperature. This χ_{0110} can be considered as a plaquette-local precursor of the d-wave superconducting instability in the plaquette-lattice.

Now we proceed to constructing the d-wave pairing operator and consequently the d-wave generalized susceptibility. The pairing operator is given by (up to a normalization factor):

$$\Delta_i^d(\nu) = \sum_j a_{ij} \Delta_{ij}^s(\nu), \quad (\text{E2})$$

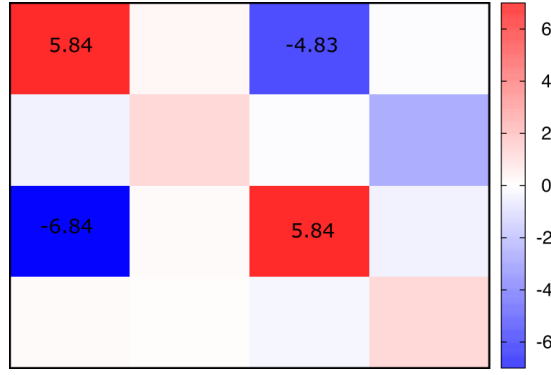


FIG. 14. Elements of particle-particle susceptibility matrix χ_{ijkl} with the fixed $(i, j) = (0, 1)$, k going from 0 to 3 from left to right and l from 0 to 3 from bottom to top.

where $a_{ij} = 1$ when ij is a horizontal bond, $a_{ij} = -1$ when it is a vertical bond, and $a_{ij} = 0$ otherwise. Thus for example $\Delta_0^d = \Delta_{03}^s - \Delta_{01}^s$. The d -wave generalized susceptibility is then given by $\chi_{ik}^d(\nu, \nu') = \langle \Delta_i^d(\nu) \Delta_k^d(\nu') \rangle$. We will be interested only in the homogeneous part of it given by:

$$\chi^d(\nu, \nu') = \sum_k \chi_{0k}^d(\nu, \nu'). \quad (\text{E3})$$

Breaking this expression into single contributions and keeping only the non-equivalent terms (in other words fixing the first pair of indices to 01) we get:

$$\chi^s = \chi_{0110}^s + \chi_{0101}^s - \chi_{0121}^s - \chi_{0112}^s + \chi_{0132}^s + \chi_{0123}^s - \chi_{0103}^s - \chi_{0130}^s. \quad (\text{E4})$$

Fig. 14 shows the elements $\chi_{01kl}^s(\nu = \pi/\beta, \nu' = \pi/\beta, \omega = 0)$ for different $k = 0 \div 3$ and $l = 0 \div 3$. We can see that all non-negligible elements coherently increase each other according to the d -wave symmetry, therefore there is no cancellation and no frustration.

Fig. 15 shows the vertex (in our case just connected correlator) $\gamma(\nu, \nu', \omega = 0)$ of the reference model as a function of inverse temperature.

Results for the maximum eigenvalues of the Bethe-Salpeter matrix Λ_{ij} for different hole doping are presented in the Fig. 16. In the half-field case with $t' = 0$ and $\mu_0 = U/2$ the main instability is related to the particle-hole magnetic channel with the eigenvector corresponding to an antiferromagnetic checkerboard structure. In this case there is no density or superconducting instability. For the optimally doped case ($\mu_0 = 0.8$) the largest instability is related to the particle-particle singlet $d_{x^2-y^2}$ superconductivity. The density instability is not robust against small change in (μ_0) for the plaquette. Finally for the overdoped case ($\mu_0 = 0.0$) there is no instability until $\beta = 10$ which may indicate a formation of a normal metallic phase.

The Fig.17 shows the periodized lattice DF plaquette self-energy according to Eq. (17) in the full Brillouin zone 64×64 \mathbf{k} -mesh for the lowest Matsubara frequency. The real part of the self-energy already has an anomalously sharp feature near X point in the Brillouin zone.

In the Fig.18 we compare the density of states (DOS) for plaquette DF perturbation for two different approximations: the table $t' = 0.15$ corresponds to $t'_0 = t' = 0.15$ and $\mu = 1.0$, while the case $t' = 0.3$ corresponds to $t' = 0.3$ with reference hopping $t'_0 = 0.15$ and $\mu = 0.7$. Both calculations correspond approximately to hole doping $\delta = 0.15$.

We plot the frequency-dependent of Σ' self-energy only within the plaquette extent (Σ') and compare to the bare plaquette reference self-energy (Σ_0) [see Eq. (17)] for two different temperatures in Fig.19 and Fig.20. Note the increase of (Σ'_{02}) (along t') with decreasing temperature already for $\beta = 5$.

Appendix F: ED for the 4×4 cluster

We analyse low-lying many-body states of the (4×4) periodic cluster for the sector $(7\uparrow, 7\downarrow)$ in Fig. 21 and indicate the degeneracy of a few important states with numbers. The ground state for $t' = 0$ is three-fold degenerate due to 2^4 super-cube symmetry⁷¹. As a function of t' this state splits to a ground state doublet and a singlet which has higher energy. Around $t'/t = -0.12$ the ground state of the sector $(7\uparrow, 7\downarrow)$ changes to a singlet (red line on the Fig. 21) with a much lower energy and different symmetry related with a drastic change of the spin-spin correlations from antiferromagnetic-like for small t' to basically nonmagnetic for larger t' (Fig. 24).

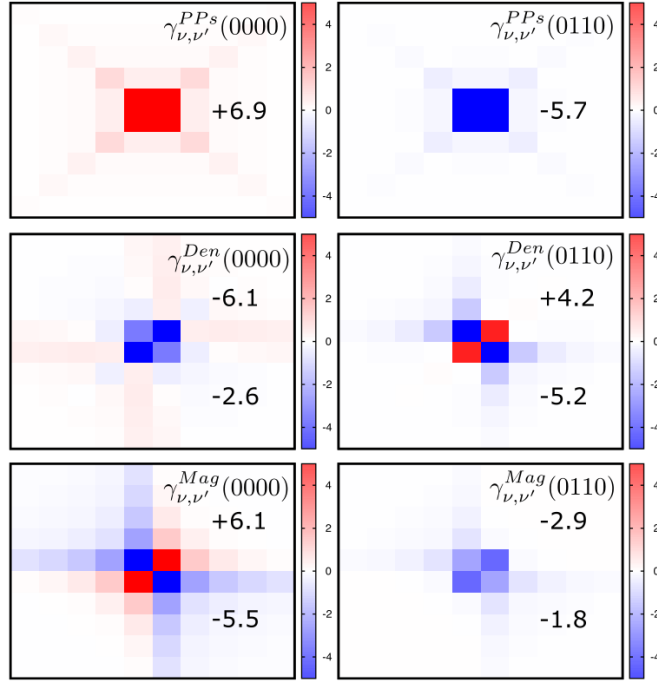


FIG. 15. Real part of Vertex function $\gamma_{\nu,\nu'}^{PP/PH}(ijkl)$ for different plaquette indices with $U=5.56$ and $t'/=-0.3t$, $\mu_c=0.479$ $\beta=10$. Maximum positive and negative values are shown

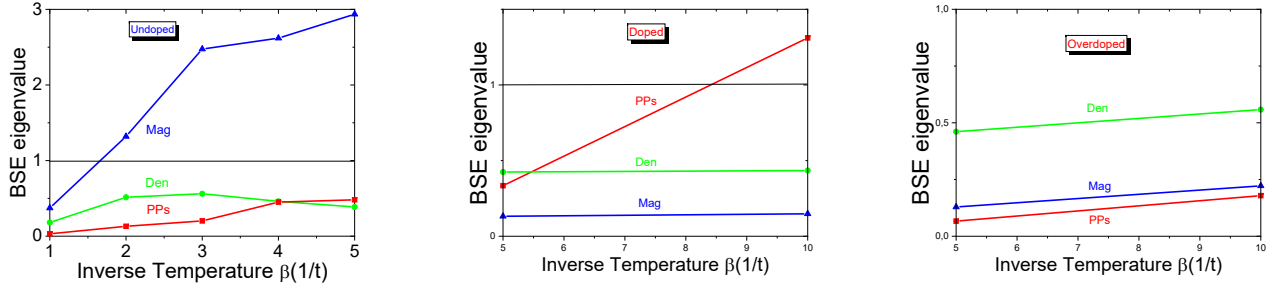


FIG. 16. Maximum eigenvalues of BSE for half-filled plaquette with $U=8$ and $t'=0$ (left), for doped plaquette with $U=5.56$ and $t'=-0.3t$, $\mu_0=0.8$ $\mu=1.55$ (middle), and for overdoped plaquette with $U=5.56$ and $t'=-0.3t$, $\mu_0=0.0$ $\mu=1.5$ (right)

Fig. 22 (left panel) shows the many-body ground state energies for (4×4) periodic cluster for different sectors with N electrons for different interaction strength $U = 0 \div 12$ (from bottom to top). One can clearly see that the largest effect of lowering energy of $N = 14$ sector compared to the half-field $N = 16$ one (red dot) appears at $U = 6$ where the pair-hole binding energy has the minimum for $t'/t = -0.3$ (Fig. 6). In the right panel of Fig. 22 we show a comparison of our exact diagonalization of the 4×4 periodic cluster for $t'/t = -0.15$ with the ED results of Dagotto et.al.⁶¹ for $t' = 0$ and $U=4, 8, 10$. Note that our ED results for $t' = 0$ exactly reproduce the ones of Dagotto et.al.⁶¹. We note that the many-body energies for the half-field cluster $N = 16$ is almost perfectly insensitive to small changes of t' due to the antiferromagnetic blocking of the t' hoppings. The same effect is observed even for the one hole case ($N = 15$), probably due to a large string-like $t - J$ blocking⁶¹. However for the two-hole situation ($N = 14$) there is clearly an appreciable lowering of ground state energy for $U = 4$ where the pair-hole binding energy has a minimum for $t'/t = -0.15$ (Fig. 6).

In Fig. 24 different static correlators are shown from ED calculations for the (4×4) periodic cluster with $t' = 0$ and $t'/t = -0.3$. The spin-spin correlators in the sector $N = 14$ ($7\uparrow, 7\downarrow$) drastically change behaviour from almost antiferromagnetic at $t' = 0$ to almost nonmagnetic structure with the weak negative correlations within the horizontal and vertical stripes. The charge-charge correlators seem to be robust against large changes of t' . The hole density correlators will be discussed below.

Fig. 27 shows the density of states for different sectors (hole concentrations) for ED calculations of (4×4) periodic cluster with $t'/t = -0.15$ and $t'/t = -0.3$. We can conclude that for $t'/t = -0.3$ and optimal $U = 5.56$ all calculated sectors corresponding to

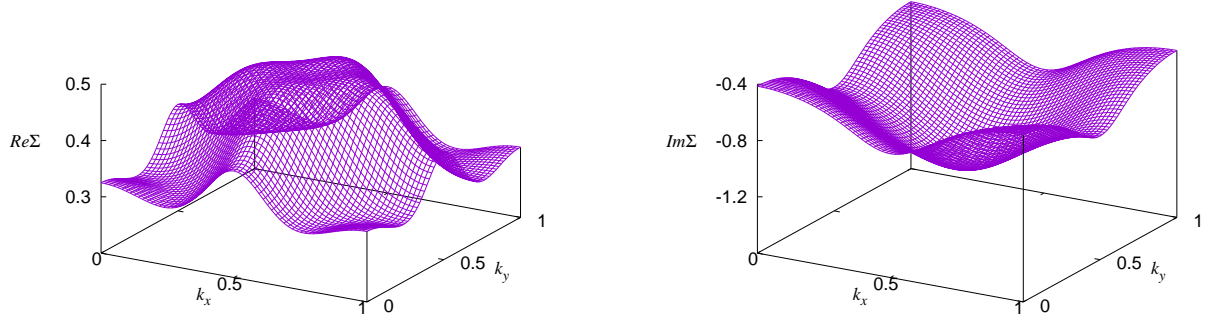


FIG. 17. Real (left) and imaginary (right) part of lattice $\Sigma_{\mathbf{k},v=\pi T}$ for dual fermion plaquette theory for $U=5.56$, $t'/t=-0.15$, $\mu_0 = 0.48$, $\mu=1.55$ and $\beta = 3$.

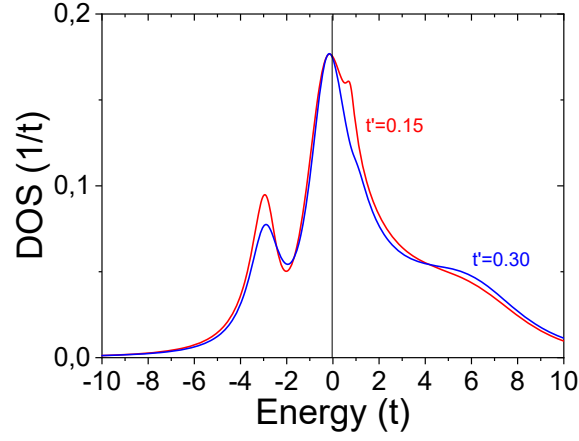


FIG. 18. Density of states for dual fermion plaquette superperturbation (DF) for $U=5.56$, $t'_0/t=-0.15$, $\mu_0 = 0.48$ in two different approximations: $t'/t=-0.15$, $\mu=1.0$ and $t'/t=-0.3$, $\mu=0.7$

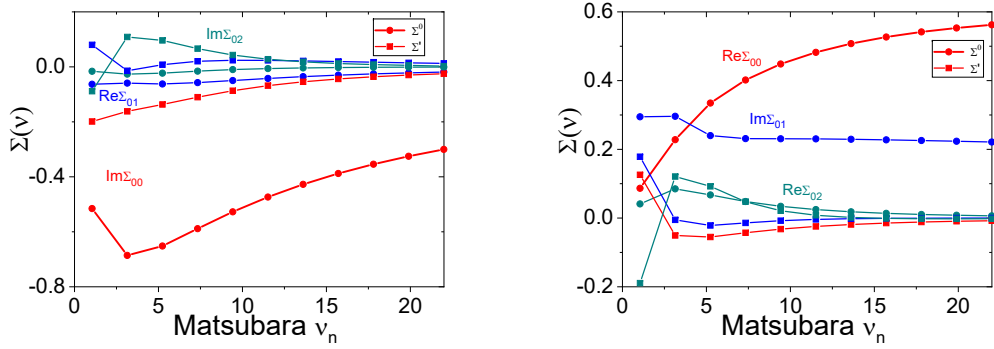


FIG. 19. Self-energy for the optimally doped case for the reference system (Σ_0 , circle) and the non-local DF part (Σ' , square) for $\beta = 3$, $\mu = 1.55$ from the plaquette DF-perturbation at the degenerate point.

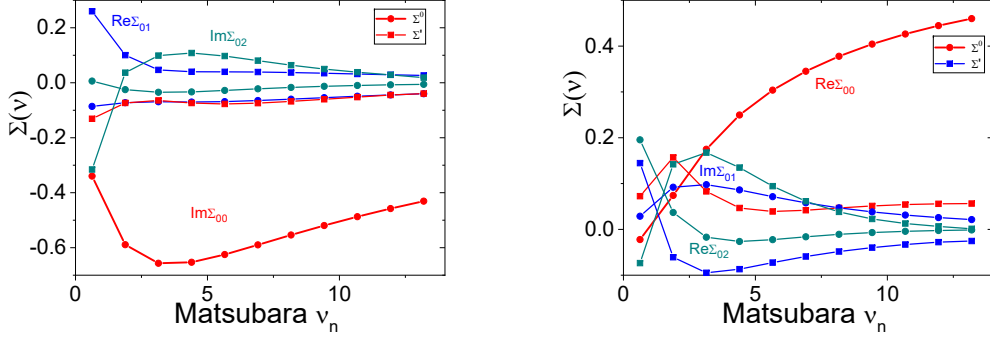


FIG. 20. Self-energy for the optimally doped case for the reference system (Σ_0 , circle) and the non-local DF part (Σ' , square) for $\beta = 5$, $\mu = 1.55$ from the plaquette DF-perturbation at the degenerate point.

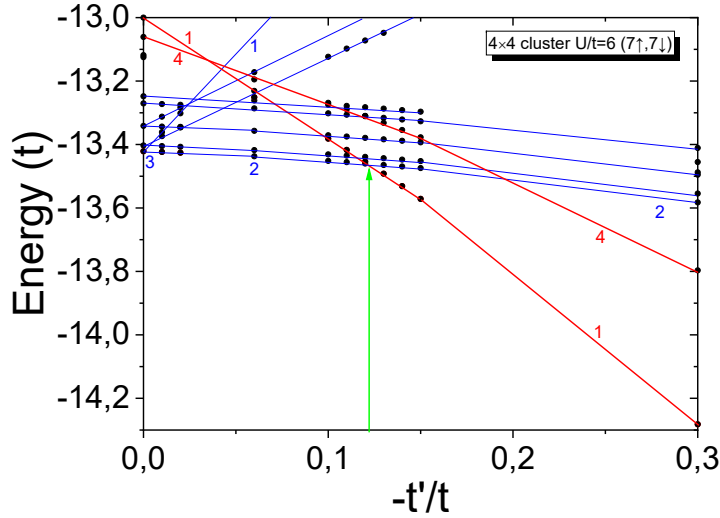


FIG. 21. Many body states of (4×4) periodic cluster for the sector $(7\uparrow, 7\downarrow)$ as a function of t' for $U/t = 6$. The degeneracy of few low-lying states are marked with the numbers. The green arrow indicate the critical t' for ground state crossing.

doping $\delta = 0.0525 \div 0.25$ have large pseudogap DOS. Simple pictorial view on such pseudogap formation presented in Fig. 29 (left). If we consider (4×4) cluster build from four interacting (2×2) plaquettes each of has sharp peak at Fermi level, then it is clear that through the resonant interactions the total DOS would have a pseudogap at E_F . This is similar to the Fano effect for Kondo-like impurity in the conducting bath.

We should point out that the optimal interaction $U/t \approx 6$ is smaller than the bandwidth $W/t = 8$ and substantially below the strong coupling, effective $t - J$ model limit. Therefore, the huge hole-hole binding we found in the 4×4 cluster at intermediate $U/t \approx 6$, with two holes located on different “diagonal” plaquettes, is very different from the so-called “string-like” effective hole-hole interactions in the $t - J$ model, where two holes are sitting with nearest-neighbor or next-nearest-neighbor distance⁶¹, i.e., in the same plaquette. In the Fig. 23 we presented the pair-hole binding energy for the ED calculations of a (2×2) periodic plaquette with $t'/t = -0.3$ as a function of U . The energy of the two-hole binding is much smaller than for (4×4) cluster with the same t' . The two-hole binding energy in a single 2×2 plaquette is very similar to the results of Ref.¹⁸ at $t' = 0$. This indicates that it is not favourable to put two holes in a single plaquette. Thus, the pairing is a phenomenon that emerges in the lattice of plaquettes, as we could also see in the dual Bethe-Salpeter equation.

It is also instructive to compare the changes in the static hopping correlator $\langle \hat{c}_0^\dagger \hat{c}_j \rangle$ within the sector $(7\uparrow, 7\downarrow)$ for different t' (see Fig. 25). While in the case of $t' = 0$ all next-nearest hoppings are very small, including of $t'/t = -0.3$ produces “long-range” hopping correlators in all directions which highlights the role of kinetic stabilization of the two-hole states.

Fig. 28 shows the \mathbf{k} -dependent self-energy from exact diagonalization for of 4×4 cluster for $\delta = 0.125$ ($7\uparrow, 7\downarrow$) with local and first three non-local elements of $\Sigma_{ij}(\nu = \pi T)$ in the real space. We cut the more long-range elements of $\Sigma_{ij}(\nu)$ in the

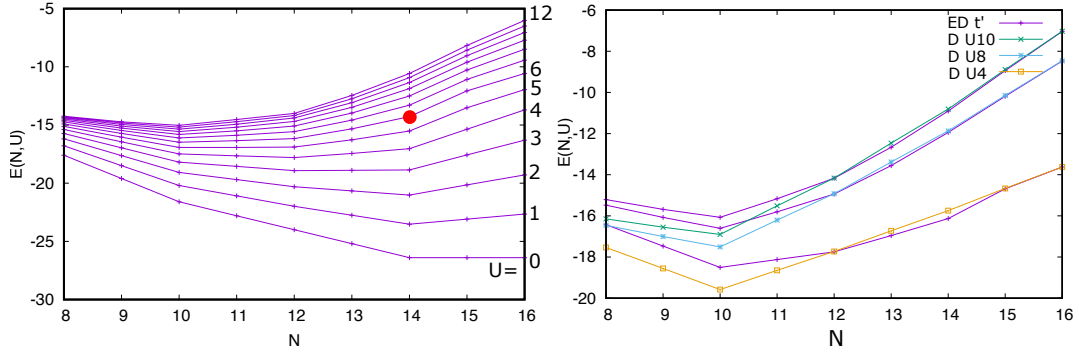


FIG. 22. Many body ground state energies of (4×4) periodic cluster for different sectors as function of U for $t'/t = -0.3$ and $\mu = 0$. The red points shows the largest effect of lowering the total energy for the sector $N = 14$ ($7\uparrow, 7\downarrow$) (left). In other words, $E(14, U) - E(16, U)$ is minimal for $U = 6$. Comparison of the present ED calculations for $t'/t = -0.15$ with (ED t') ED results of Dagotto et.al⁶¹ for $U=4, 8, 10$ from bottom to top (right).

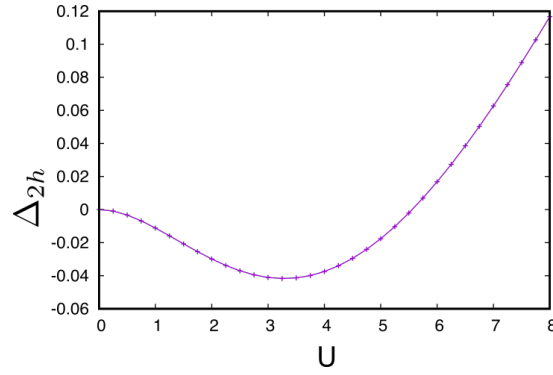


FIG. 23. Energy of two-hole binding for 2×2 plaquette for $t'/t = -0.3$. Note that the energy scale is reduced by more than an order of magnitude compared to the 4×4 plaquette, see Fig. 6.

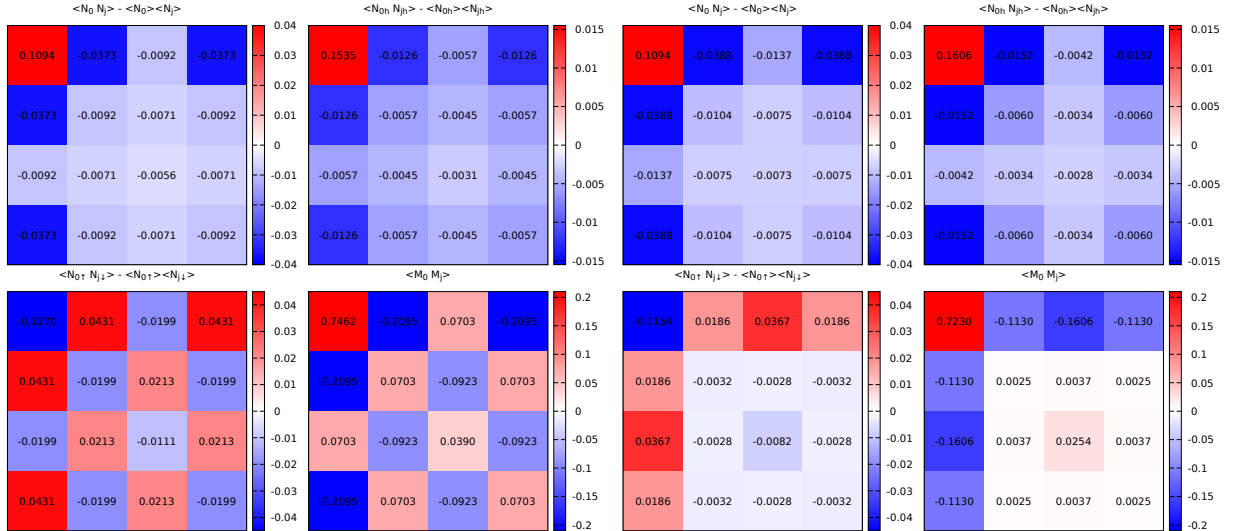


FIG. 24. Different Static correlators of the ground state of the (4×4) periodic cluster for the sector $(7\uparrow, 7\downarrow)$ for $U/t = 5.56$ and $t'/t = 0$ (left) and $t'/t = -0.3$ (right).

Fourier transform due to periodic boundary condition. The general shape of the self-energy agree well with results of plaquette DF-perturbation (Fig. 17).

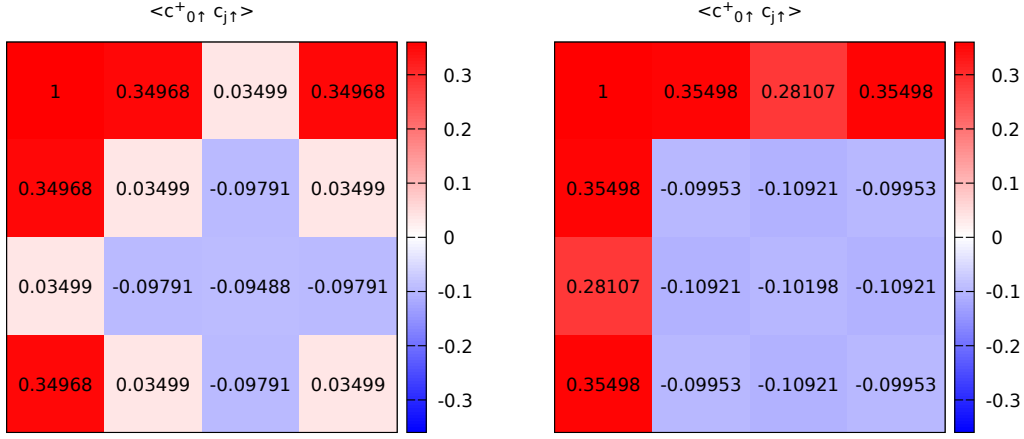


FIG. 25. Static correlators: $\langle 7 \uparrow, 7 \downarrow | \hat{c}_0^\dagger \hat{c}_j | 7 \uparrow, 7 \downarrow \rangle$ of (4×4) periodic cluster for the sector for $U/t = 5.56$ and $t'/t = 0$ (left) and $t'/t = -0.3$ (right).

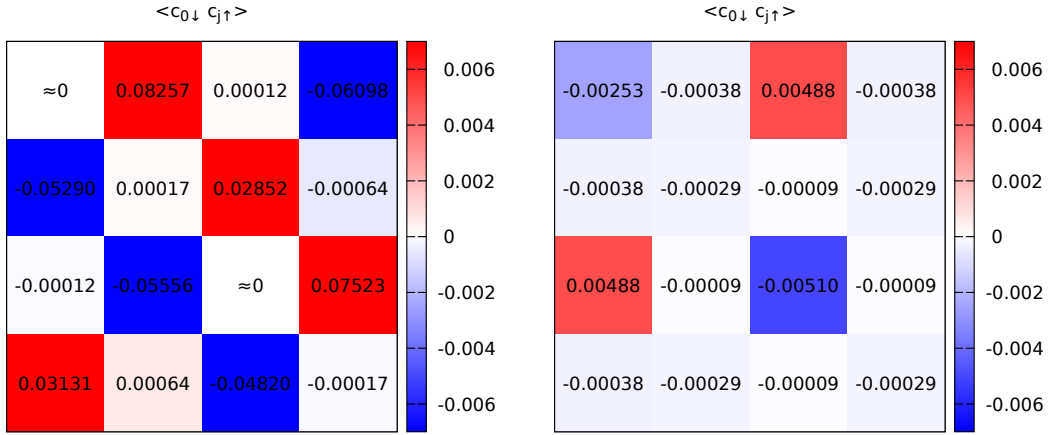


FIG. 26. Static correlators: $\langle 7 \uparrow, 7 \downarrow | \hat{c}_0 \hat{c}_j | 8 \uparrow, 8 \downarrow \rangle$ of (4×4) periodic cluster for the sector for $U/t = 5.56$ and $t'/t = 0$ (left) and $t'/t = -0.3$ (right).

Appendix G: Hole-hole correlation in 4×4 plaquette

To investigate the important issue of the hole-hole interaction in the lattice, we use two approaches to the notion of a hole in the 4×4 plaquette. The first one is to consider a hole as an absence of electrons, *i.e.*, an empty site is viewed as a hole. The hole density operator at site i is then given by

$$n_i^h = (1 - n_{i\uparrow})(1 - n_{i\downarrow}). \quad (G1)$$

We then investigate the hole-hole correlation function $\langle n_i^h n_j^h \rangle - \langle n_i^h \rangle \langle n_j^h \rangle$ in the ground state of the $(7\uparrow, 7\downarrow)$ sector as a function of the displacement $i - j$. The average hole density $\langle n_i^h \rangle$ is obviously given by $\langle n_i^h \rangle = 1 - \langle n \rangle + d$, where $\langle n \rangle$ is the average electron density, which in the given sector is just $7/8 = 0.875$, and $d = \langle n_{i\uparrow} n_{i\downarrow} \rangle$ is the double occupancy. The results for two different values of t' are shown in Fig. 24.

The analysis of the hole-hole correlation function in this sector shows that the two holes occupy two different plaquettes in 4×4 cluster with a slight tendency towards “diagonal” plaquettes, or in other words the holes prefer to be as far from each other as the system permits. Energetically, this configuration of the holes makes the t' hopping along the diagonals very efficient (see also Fig. 29 (right)). Thus, it is the kinetic energy associated with t' which drives such a strong hole-condensation for this concentration $\delta = 0.125$ (2 holes on 16 sites), which is not far from the optimal hole concentration for cuprates.

The second approach is in the spirit of Landau’s Fermi liquid theory. The hole is then viewed as the result of an annihilation operator acting on the half-filled $((8\uparrow, 8\downarrow)$ sector) ground state $|\psi_{16,0}\rangle$. Correspondingly a state with two holes would be the result

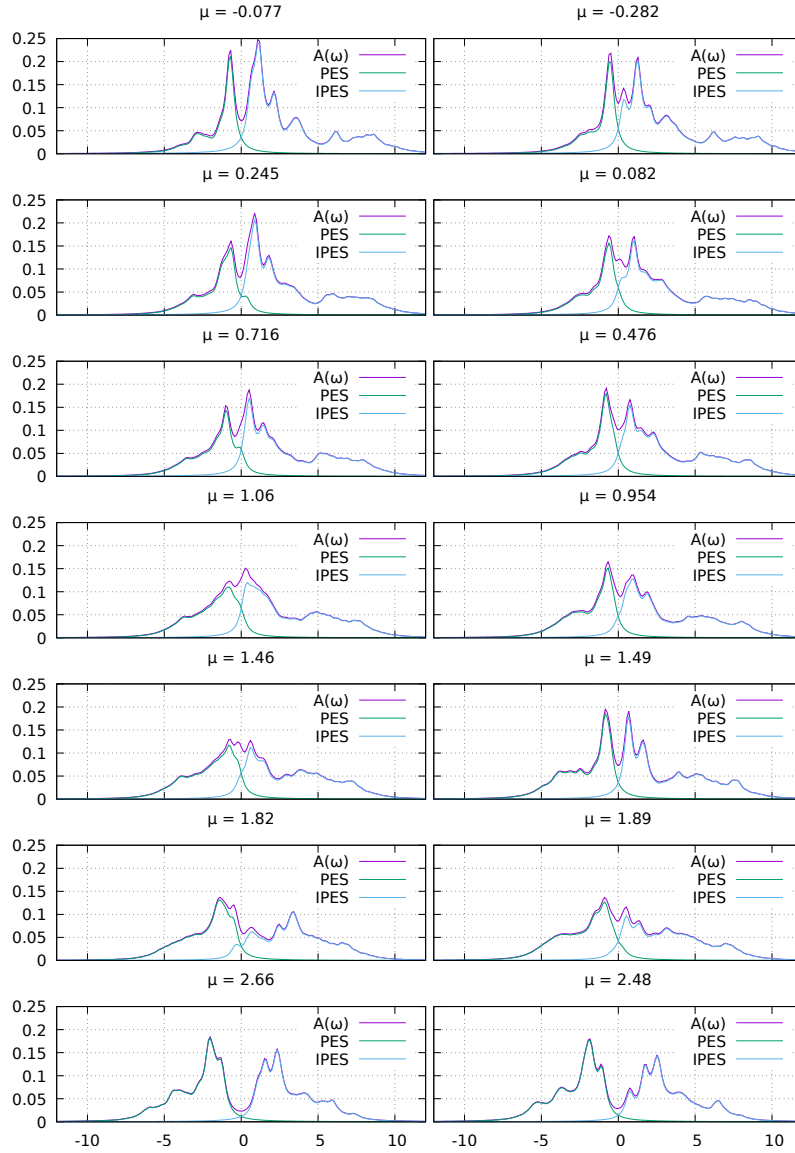


FIG. 27. DOS for (4×4) periodic cluster $\beta = 10$ Spectral density $A(\omega)$ (as well as PES and IPES part) of periodic 4×4 cluster with $U=5.56$, $\beta = 10$ and different NNN hopping t' : 0.15 (left column), 0.3 (right column). Different doping and corresponding sectors are shown from the top to bottom: $\delta = 0.375$ ($5\uparrow, 5\downarrow$); $\delta = 0.3125$ ($6\uparrow, 5\downarrow$); $\delta = 0.25$ ($6\uparrow, 6\downarrow$); $\delta = 0.1875$ ($7\uparrow, 6\downarrow$); $\delta = 0.125$ ($7\uparrow, 7\downarrow$); $\delta = 0.0525$ ($8\uparrow, 7\downarrow$), $\delta = 0$ ($8\uparrow, 8\downarrow$).

of two annihilation operators acting on that state: $|\psi_{14;ij}\rangle = A_{ij}c_{i\uparrow}c_{j\downarrow}|\psi_{16;0}\rangle$, with A_{ij} being the normalization factor chosen in such a way that the norm of this state is unity. Then we calculate the overlap C_{ij} between the ground state of the $(7\uparrow, 7\downarrow)$ sector $|\psi_{14;0}$ and $|\psi_{14;ij}\rangle$ to see how well the two-hole state describes the true ground state. The results are shown in Fig. 26. Here we have to understand that for $t' = 0$ the ground state of the 4×4 plaquette is 3 fold degenerate. This is an accidental degeneracy that occurs because the 4×4 periodic lattice without t' is equivalent to a $2 \times 2 \times 2 \times 2$ hypercubic lattice⁷¹. This accidental degeneracy is unphysical in the sense that it is absent in larger two-dimensional clusters. Other effects of this property one can see on the left panel of fig. 24 noting that observables when i and j are nearest neighbors along the diagonal are identical with those when i and j are next nearest neighbors along the horizontal or vertical direction. On a 4-dimensional hypercube those pairs of sites are equivalent.

Due to this degeneracy and to the fact that C_{ij} is not an observable we have to take the results for $t' = 0$ with a grain of salt. The results are obviously dependent on the linear combination of the three ground states we choose to calculate the overlap (fig. 24 shows one such combination produced randomly by the ED solver). Still, we can see that C_{ij} tends to be largest if i and j have different spins on the Néel state. This is a clear indication that antiferromagnetic fluctuations are well preserved in the $(7\uparrow, 7\downarrow)$ sector with no NNN hopping. On the other hand for $t' = 0.3$ the largest overlap is found for the pairs (1,3) and (1,11), sites being numbered from 1 to 16 from left to right and then from top to bottom, in agreement with the understanding that large

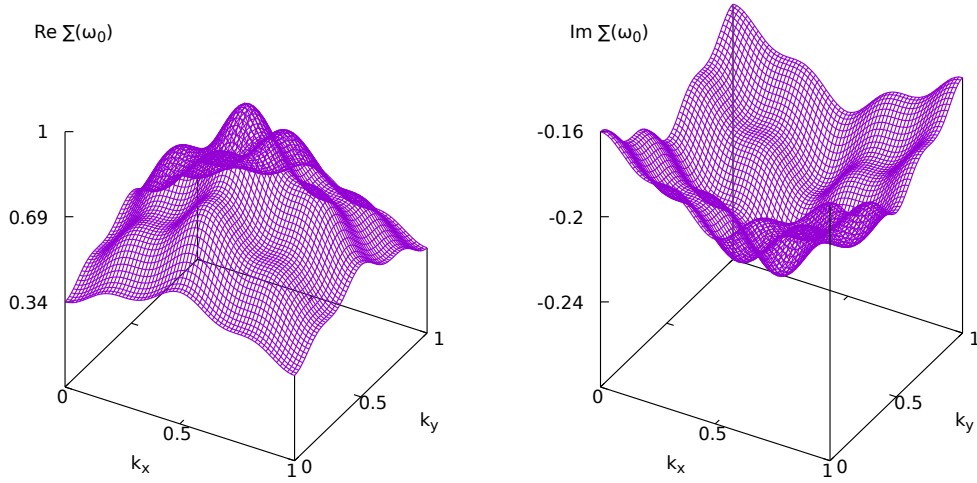


FIG. 28. Real (left) and imaginary (right) part of self-energy $\Sigma_{\mathbf{k}, \nu=\pi T}$ in Brillouin zone from exact diagonalization of 4×4 cluster for $U = 5.56$, $t'/t = -0.3$, $\beta = 10$ and $\delta = 0.125$ in the $(7\uparrow, 7\downarrow)$ sector.

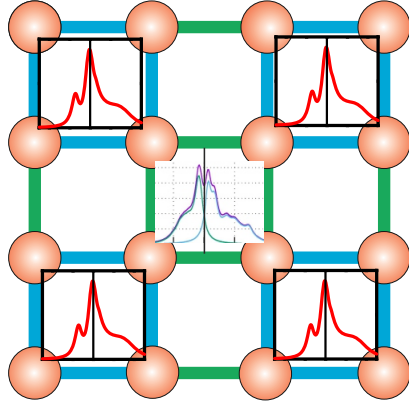


FIG. 29. Schematic view of pseudogap formation in (4×4) periodic cluster from the peak DOS structure of individual 2×2 plaquettes.

NNN hopping completely destroys the antiferromagnetic order.

Another interesting observation arises when we calculate the sum $\sum_{ij} C_{ij}^2$ for different values of t' . This value shows how well the $|\psi_{14,0}\rangle$ state is described in terms of the two holes states $|\psi_{14,ij}\rangle$. It turns out that while for $t' = 0$ this value is reasonably large (1.25, one should be surprised it is larger than one as the states $\Psi_{14,ij}$ are not orthogonal), for $t' = 0.3$ it is very low (0.0013). This indicates that the second approach to the notion of hole, in terms of the Fermi liquid theory is hardly appropriate for large t' , in other words the holes in that regime are very incoherent.

Appendix H: Lehmann representation for one-particle and two-particle Green's functions

The one-particle Green's function for a finite fermionic system with time-independent Hamiltonian and many body spectrum $\hat{H}|i\rangle = E_i|i\rangle$ has the following Lehmann representation in the Matsubara space:

$$g_{12}^{\sigma}(v) = \frac{1}{Z} \sum_{ij} \frac{\langle i | \hat{c}_{1\sigma} | j \rangle \langle j | \hat{c}_{2\sigma}^{\dagger} | i \rangle}{iv + E_i - E_j} (e^{-\beta E_i} + e^{-\beta E_j})$$

where $Z = \sum_i e^{-\beta E_i}$.

For the two-particle Green's function (2PGF) we introduce first four "auxiliary" fermionic frequencies $(\omega_1 \div \omega_4)$ and define 2PGF in Matsubara space as following⁴⁸:

$$\kappa_{1234}^{\sigma\sigma'}(\omega_1\omega_2\omega_3) = \frac{1}{\beta^2} \int_0^{\beta} d\tau_1 \int_0^{\beta} d\tau_2 \int_0^{\beta} d\tau_3 e^{i(\omega_1\tau_1 + \omega_2\tau_2 + \omega_3\tau_3)} \langle T_{\tau} c_{1\sigma}(\tau_1) c_{2\sigma'}(\tau_2) c_{4\sigma'}^{\dagger}(\tau_3) c_{3\sigma}^{\dagger}(0) \rangle. \quad (\text{H1})$$

Here time translation invariance of the imaginary time 2PGF has been used. Note that here the frequencies in the exponential corresponding to annihilation and creation operators have the same sign in contrast to the usual definition for the Fourier transform. Correspondingly, energy conservation requires $\omega_1 + \omega_2 + \omega_3 + \omega_4 = 0$. By restricting the range of integration such that time ordering is explicit, one obtains 3! different terms. These can be brought into the same form by permuting the operators and corresponding frequencies. By the anticommutation relations, each term picks up the sign of the permutation. After introducing the sum over eigenstates, the 2PGF can be written as

$$\kappa_{1234}^{\sigma\sigma'}(\omega_1\omega_2\omega_3) = \frac{1}{Z} \sum_{ijkl} \sum_{\Pi} \phi(E_i, E_j, E_k, E_l, \omega_{\Pi_1}, \omega_{\Pi_2}, \omega_{\Pi_4}) \text{sgn}(\Pi) \langle i | O_{\Pi_1} | j \rangle \langle j | O_{\Pi_2} | k \rangle \langle k | O_{\Pi_4} | l \rangle \langle l | c_{3\sigma'}^\dagger | i \rangle \quad (\text{H2})$$

where the first sum is over the eigenstates and the second over all permutations Π of the indices $\{123\}$. We further have defined $O_1 = c_{1\sigma}$, $O_2 = c_{2\sigma'}$ and $O_4 = c_{4\sigma'}^\dagger$ and e.g. Π_1 denotes the permutation of the first index. Here the different choice of convention for the Fourier transform simplifies the notation since otherwise the sign of the frequency associated with the creation operator would have to be permuted. The function ϕ is given by the integral

$$\phi(E_i, E_j, E_k, E_l, \omega_1, \omega_2, \omega_3) = \int_0^\beta d\tau_1 \int_0^{\tau_1} d\tau_2 \int_0^{\tau_2} d\tau_3 e^{-\beta E_i + (E_i - E_j)\tau_1 + (E_j - E_k)\tau_2 + (E_k - E_l)\tau_3 + i(\omega_1\tau_1 + \omega_2\tau_2 + \omega_3\tau_3)} \quad (\text{H3})$$

The latter expression can be evaluated by taking care of the delta functions that arise from equal energies, with the final result⁴⁸:

$$\begin{aligned} \phi(E_i, E_j, E_k, E_l, \omega_1, \omega_2, \omega_3) &= \frac{1}{i\omega_3 + E_k - E_l} \times \\ &\left[\frac{1 - \delta_{\omega_2, -\omega_3} \delta_{E_j, E_l}}{i(\omega_2 + \omega_3) + E_j - E_l} \left(\frac{e^{-\beta E_i} + e^{-\beta E_j}}{i\omega_1 + E_i - E_j} - \frac{e^{-\beta E_i} + e^{-\beta E_l}}{i(\omega_1 + \omega_2 + \omega_3) + E_i - E_l} \right) \right. \\ &+ \delta_{\omega_2, -\omega_3} \delta_{E_j, E_l} \left(\frac{e^{-\beta E_i} + e^{-\beta E_j}}{(i\omega_1 + E_i - E_j)^2} - \beta \frac{e^{-\beta E_j}}{i\omega_1 + E_i - E_j} \right) - \frac{1}{i\omega_2 + E_j - E_k} \times \\ &\left. \left(\frac{e^{-\beta E_i} + e^{-\beta E_j}}{i\omega_1 + E_i - E_j} - (1 - \delta_{\omega_1, -\omega_2} \delta_{E_i, E_k}) \frac{e^{-\beta E_i} - e^{-\beta E_k}}{i(\omega_1 + \omega_2) + E_i - E_k} + \beta e^{-\beta E_i} \delta_{\omega_1, -\omega_2} \delta_{E_i, E_k} \right) \right]. \end{aligned} \quad (\text{H4})$$

Finally connection to standard Matsubara frequencies in 2PGF used in this work is as follows:

$$\omega_1 = \nu, \quad \omega_2 = \omega - \nu, \quad \omega_3 = \omega - \nu' \quad (\text{H5})$$

There is an efficient open source implementation `pomero1`⁴⁶ for extracting the two-particle Green's function in ED.

# States	256	22	13	9	6
$\kappa_{0110}^P(\nu_0, -\nu_0, \omega = 0)$	10.75	10.51	9.62	9.58	8.02

TABLE I. The main non-local contribution to two-particle plaquette Green function at the degenerate point for PP singlet channel as function of number of included states in the Lehmann representation for $\beta = 10$. See Fig. 4 for other parameters.

Using the Lehmann representation Eq. (H1) we can analyze effects of the 6-fold degenerate ground states for the "critical" point on the plaquette on the values of the two-particle Green function. In the 4-fold sum over all many body states $ijkl$ one can reduce only one summation using the low-temperature limit related with a cutoff due to the Boltzmann factors in Eq. (H4). In order to understand effects of ground state degeneracy, we can formally reduce sum over *all* many body states over the lowest N -states. In the Table I we presented the main non-local contribution to two-particle plaquette Green function for PP singlet channel $\kappa_{1221}^P(\nu_0, -\nu_0, \omega = 0)$ as function of number of included states in the Lehmann representation. If we include all 256 states for $\beta = 10$ in the 2×2 plaquette then we get exactly the value of particle-particle singlet susceptibility (10.75) in the Fig. (13) for this inverse temperature. We note that there is no disconnected part and susceptibility is equal to κ^P in this channel. It is interesting than using only the 6 degenerate ground states states gives about 75% of the total value for $\kappa_{1221}^P(\nu_0, -\nu_0, \omega = 0)$ which is a "main contribution" for $d_{x^2-y^2}$ superconductivity. Moreover taking into account only 3 additional states at the energy $E_n = 0.42$ from $N = 4$ triplet, the summation over 9 low-energy many-body states in plaquette gives about 90% of the total values. This test clearly shows importance of the ground states degeneracy in the special point of plaquette with $\delta = 0.25$ for divergence of renormalized vertex for lower temperature in the dual-fermion perturbation theory.